Chapter 1
Ligand-Free Sub-Nanometer Metal Clusters in Catalysis

Judit Oliver–Meseguer and Antonio Leyva–Pérez

Abstract Recent advances in the synthesis and characterization of ligand-free sub-nanometer metal clusters, either in solution or supported on solids, have enabled their rational use as catalysts in new reactions. These clusters expose all their metal atoms to outer molecules without the potential steric/electronic interferences of ligands, while, at the same time, show defined molecular orbitals to ultimately control the catalytic reaction. Therefore, these clusters somehow combine the advantages of single atom and metal nanoparticles for molecular activation and catalysis. This chapter aims at describing how to prepare, better characterize and apply, on a realistic scale, ligand-free sub-nanometer metal clusters for catalytic processes (many of them of industrial interest) during the last ten years.

Keywords Sub-nanometer metal clusters · Catalysis · Ligand-free · Industrial reactions

1.1 Introduction

1.1.1 History and Nanotechnology Projection

The prefix *nano* gives the name to a discipline that is considered the scientific sign of our generation, the nanotechnology, although this is not a novelty for humanity. The book written by the philosopher and medical doctor Francisci Antonii in 1618, *Aurea–Auro Potabile*, is considered as the first book on colloidal Au. The reputation of soluble Au until the Middle Ages was to disclose fabulous curative powers for various diseases, such as heart and venereal problems, dysentery, epilepsy and tumors and for diagnosis of syphilis. Also, this book includes considerable information on the formation of colloidal Au solutions and their medical uses, including successful practical cases (Fig. 1.1), whereas the extraction of Au started in the 5th millennium

J. Oliver–Meseguer · A. Leyva–Pérez (✉)
Instituto de Tecnología Química (UPV–CSIC), Universitat Politècnica de València–Consejo Superior de Investigaciones Científicas, Avda. de Los Naranjos s/n, 46022 València, Spain
e-mail: anleyva@itq.upv.es

P. W. N. M. van Leeuwen and C. Claver (eds.), *Recent Advances in Nanoparticle Catalysis*, Molecular Catalysis 1, https://doi.org/10.1007/978-3-030-45823-2_1


FRANCISCI ANTONII
PHILOSOPHI ET MEDICI
LONDINENSIS
PANACEA
AUREA
SIVE
Tractatus duo de ipsius
AURO POTABILI,
Nunc primum in Germania ex Londinensi Exemplari excusi,
Operâ
M. B. F. B.
JACOBUS SERENISS. REX ANGL.
Numquid ego ANTONIUM puniam, quia Deus illi benedixit.
HENR. NOLLIUS.
MEDICINAM UNIVERSALEM negant multi, sed ij plerumq; id faciunt, qui ipsam assequi non valent.
HAMBURGI
Ex Bibliopolio FROBENIANO.
ANNO CIↃ IↃ CXIIX.

Fig. 1.1 Extraction of the Panacea aurea, sive, Tractatus duo de ipsius auro potabili, from Francisci Antonii

B.C. near Varna (Bulgaria) and reached 10 tons per year in Egypt around 1200–1300 B.C., when the marvelous statue of Touthankamon was constructed, it is probable that "soluble" Au appeared around the 5th or 4th century B.C. in Egypt and China [11].

Thus, the discovery of nanoparticles was not a novelty in modern times, the merit was to discover that they were here. In 1857, Faraday used for the first time the concept nanoparticle [16], and we had to wait one century for the development of the nanotechnology after the improvement of the instruments that give access to the nanometric scale, like the scanning tunneling microscope (STM), promoted by Gerd Binning and Heinrich Rörher in 1982 (Nobel Prizes awarded in 1986) and the atomic force microscope (AFM), developed also by Binning with Christoph Gerber and Calbin Quate in 1987. Two years later, Don Eigler and Erhard Schweizer wrote the letters IBM (where they worked) manipulating 35 Xenon atoms on a Ni surface, showing the possibility to move atoms from a surface using the tip of the STM (Fig. 1.2).

1.1.2 Differences Between Nanoparticles and Sub-Nanometer Clusters

A nanoparticle is every particle with dimensions between 1 and 10^3 nm (Fig. 1.3). The chemical properties of these nanoparticles depend not only on the type of constituent

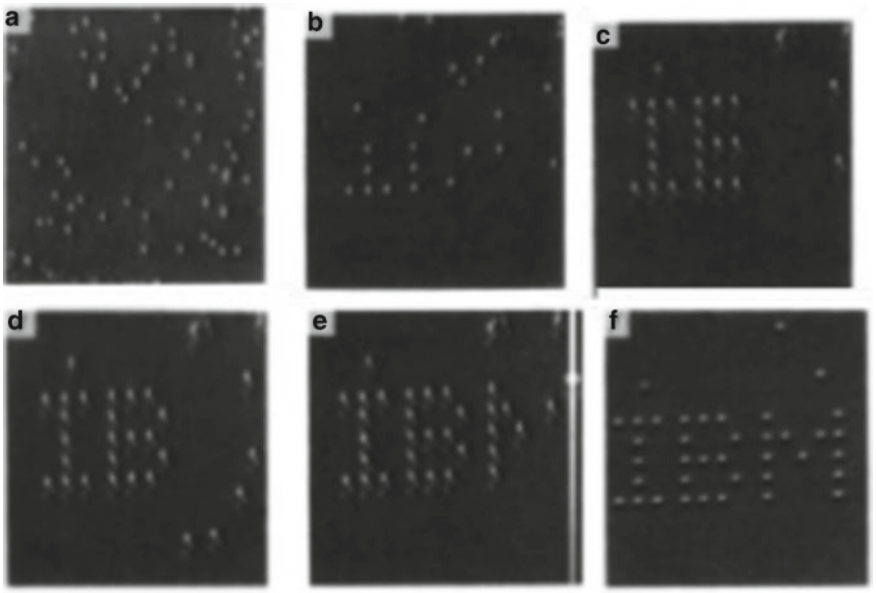

Fig. 1.2 A sequence of STM images taken during the construction of a patterned array of xenon atoms on a nickel (1 1 0) surface. The atomic structure of the nickel surface is not resolved. The h1 1 0i direction of the surface runs vertically. **a** The surface after xenon dosing, **b–f** various stages during the construction of the word IBM. Each letter is 50 (Å) from top to bottom

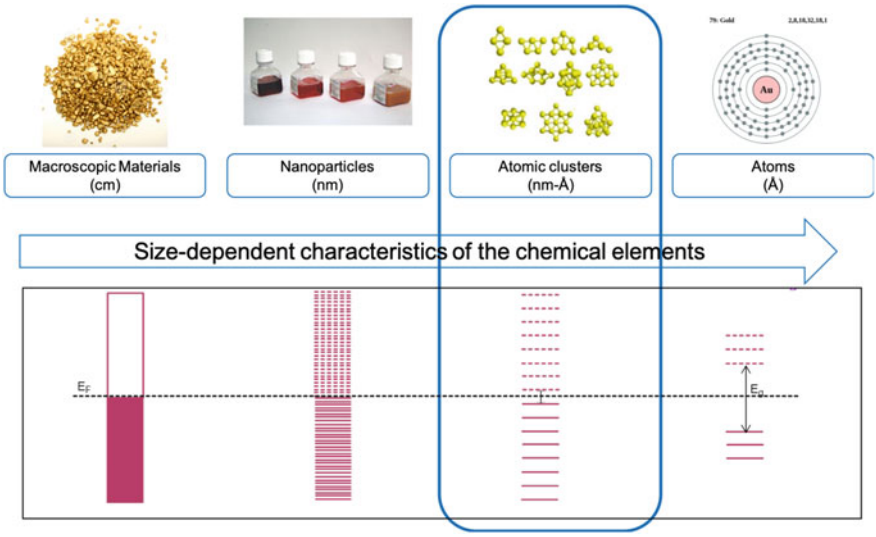

Fig. 1.3 Scheme of the size-dependent characteristics of metallic chemical elements, here illustrated for gold

atoms but also on the relationship surface/volume, the size and shape and the oxidation state, among other parameters. In the case of metallic nanoparticles, the most relevant characteristic is the plasmon. Bulk plasmons are quantum waves from electrons that are produced when the electrons are perturbed with an incident beam, changing the equilibrium position and vibrating in a given characteristic frequency. In other words, the plasmon is a collective oscillation of the conductive electrons that are shining by an appropriate wavelength.

Metal clusters are extremely small particles with a diameter less than 1 nm. Because of that, they are located between the bulk and atomic states of the corresponding metal. Due to the possibility to observe finite-size effects on the physical properties of metal clusters and to understand their microscopic origins, they have attracted physicists over the last four decades. Development of new experimental and theoretical methods has led to a discovery of a variety of remarkable size-specific phenomena and physicochemical properties. During this development, the community has come to be convinced that metal clusters are promising functional units of novel materials and has tried to develop cluster-based materials using "small is different" and "every atom counts" claims [18, 67].

1.1.3 Jellium Model

The characteristic features of small metal clusters, like the electronic shell structure and band gap, can be well understood in terms of quantum motion of the delocalized valence electrons and positively charged ionic core. This concept, known as the Jellium model for neutral metal clusters, can also be applied to charged systems [58].

This model was developed initially for clusters in the gas phase, and the cluster is replaced by an electronic structure in layers that consists of spherical Jellium (UEG—Uniform Electron Gas or HEG—Homogeneous Electron Gas) positively charged and surrounded by electrons. It is considered that the electrons move in a medium field potential occupying, according to the Aufbau principle, energy levels. This model represents a good approximation since it preserves most of the physicochemical characteristics of the clusters. The total energy, as a function of the cluster size, can be calculated by the approximation that represents the covered electronic levels and corresponds with the most stable clusters that possess the "magic numbers."

Density functional theory calculations to determine the geometric structures of the metal clusters are often used to confirm the experimental data and approximations used by the Jellium model. In general, these studies demonstrate also that there is an oscillation in the stability and the electronic properties of the clusters in function of the atom numbers, neutral clusters with odd number of atoms being more stable than ionic clusters with even atoms.

For all this, the Jellium model provides a good approximation to the electronic behavior of the clusters, describing the dependency of the photoemission energy with the number of atoms in the cluster and following Eq. 1.1:

$$E = \frac{E_F}{N^{1/3}} \tag{1.1}$$

where N is the number of the atoms in the cluster, E_F is the Fermi energy of the metal (tabulated) and E is the band gap energy, which can be approximated to the emission band in the photoluminescence experiments. With this formula in hand, it is possible to calculate the number of atoms of an unknown cluster from a simple photoluminescence spectrum.

1.2 Synthesis and Characterization of Ligand-Free Metal Clusters

When Faraday treated (gold chloride) with phosphorus to generate particles, in what he called "activated Au," he had the intuition to propose that the red-colored Au was in the form of very small particles and that the color may vary as a function of the size, something later found to be correct. Faraday's aggregates were in turn Au nanoparticles, which are still prepared today from a similar reduction procedure. Although speculative, it is possible that Faraday obtained clusters in his more diluted experiments since Au clusters are able to persist in nanomolar aqueous solutions.

There are two paths to prepare metal clusters (Fig. 1.4). In the bottom–up way, the metal clusters are prepared starting from small aggregate or single atoms, like metal complexes or salts. On the contrary, in the bottom–down path, the starting materials are bigger nanoparticles from which one can leach small aggregates of the metal.

The synthesis of large-scale metal clusters with atomic precision has experienced great advances during the last years; [32] however, most of the methods still rely on extremely expensive techniques that only recently start to be replaced by affordable wet procedures, with potential industrial application.

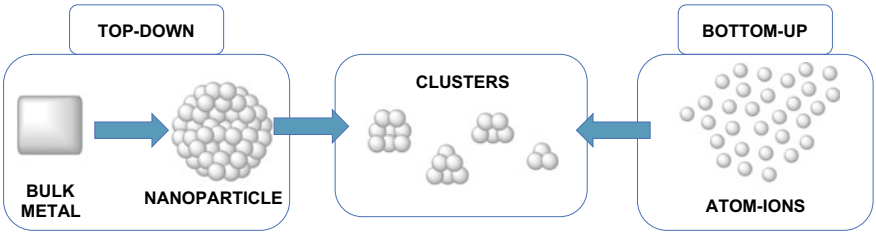

Fig. 1.4 Top–down and bottom–up approaches for the synthesis of atomic metal clusters

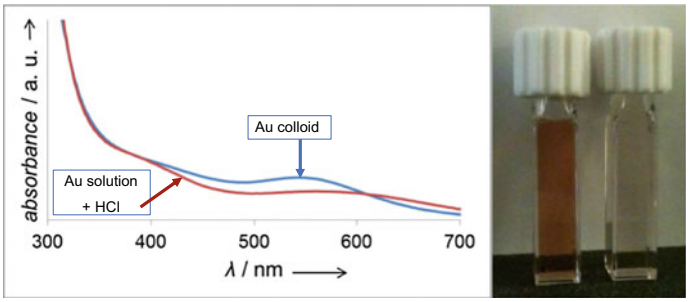

Fig. 1.5 UV/Vis spectra of the Au colloid before and after the addition of HCl and corresponding photograph (Fig. adapted from Ref. [53]. Copyright © 2013 by John Wiley & Sons, Inc.)

1.2.1 Synthesis of Metal Clusters in Solution

A first synthetic method to prepare sub-nanometric metal clusters in solution, without the aid of ligands, consists in the electrochemical etching of metallic plates in high-diluted solutions (10^{-6} M) with typical yields less than 5%. More recently, chemical methods relying on the wet reduction of a metal salt or complex with soft reduction agents (amides solvents, H_2,…) have been described [2, 7, 49, 50, 52, 53, 54, 56, 58, 59, 65]. Specifically, Au, Pd, Ag, Rh, Cu and Pt clusters between 3 and 15 atoms can be formed in reductive conditions starting from the corresponding salts and complexes. Both the electrochemical and the wet chemical methods must be carried out in very diluted solutions to avoid later agglomeration of the clusters. These diluted clusters are very useful in reactions where the amount needed to perform the catalysis is low (a few part per million, ppm, or even part per billion, ppb, amounts).

Following a top–down method, it is possible to prepare Au clusters starting from bigger nanoparticles (5–10 nm) in acid media, preferentially HCl solutions [53]. The red–purple previous aqueous colloidal solutions turn transparent after acid treatment (Fig. 1.5). UV/Vis measurements confirmed the formation of small atom Au clusters after the addition of HCl and the complete absence of the original plasmon band at approximately 550 nm.

1.2.2 Synthesis of Supported Metal Clusters

Metal clusters are formed from suitable precursors supported on solids. As it occurs in solution, these supported metal clusters can be prepared either by bottom–up or top–down approaches [3].

Following bottom–up approaches (Fig. 1.6), different solid supports have been employed, including polymers, inorganic oxides, metal-organic frameworks (MOFs), mesoporous carbon and zeolites. For instance, the bio-compatible ethylene–vinyl alcohol (EVOH) copolymer encapsulates and mildly reduces either Au, Pd, Pt or Cu

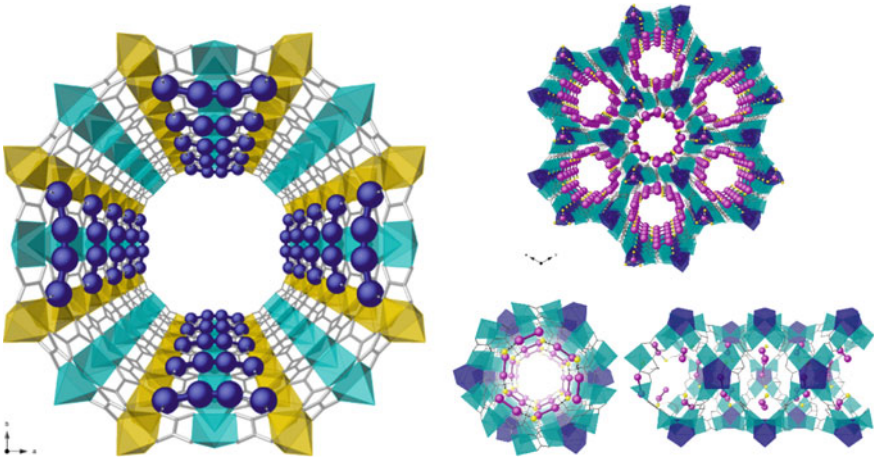

Fig. 1.6 Pd_4 (left) and Pt_2 clusters in MOFs. Metal ions of the whole net have been depicted as yellow, light and dark blue forms and ligands as gray sticks (adapted from Refs. [45 and 60]. Copyrights © 2018 by John Wiley & Sons, Inc.)

metal salts inside the polymer matrix, to give sub-nanometer clusters [17, 51, 54]. Another example of bottom–up approach is the synthesis and determination of Au clusters supported on nanoceria ($n$$CeO_2$). $n$$CeO_2$ has a high number of vacancies to stabilize catalytically active Au species, and the amount and nature of these Au species depend on the metal precursor and the reducing treatment employed. Hydrogenation at 200 °C of $n$$CeO_2$ properly impregnated with $HAuCl_4$ gives up to 15% of cationic few-atom Au clusters. For nanoporous materials, it is possible to achieve the multigram-scale chemical synthesis of up to 8 wt% sub-nanometer clusters of Pd_4 or Pt_2 on different MOFs. The synthesis of this kind of materials involves three steps: First, a robust and water-stable 3D MOF is prepared; [25, 44] then, Pd^{2+} or Pt^{4+} cations are incorporated either by anchoring the metal salt in thioether arms or by cationic exchange, and finally, the Pd_4 or Pt_2 units are obtained by reduction with $NaBH_4$. Complementary, nanoporous zeolites can also be used to synthesize well-dispersed Pt and Pd di and trinuclear clusters, with an exquisite control of the Lewis acidity [61]. Also, mesoporous carbon is a good support to stabilize monodispersed zero-valent $Pt_{5–12}$ clusters prepared from reduction of Pt–thiolate complexes, inaccessible by chemical methods [31]. In order to obtain a precise size of the metal clusters, soft-landing techniques are used in combination with gas-phase cluster ion sources and mass spectrometry. This approach is particularly effective for investigations of small nanoclusters (less than 20 atoms), where the rapid evolution of the atomic and electronic structure makes it essential to have precise control over cluster size. Cluster deposition allows for independent control of cluster size, coverage and stoichiometry (e.g., the metal-to-oxygen ratio in an oxide and oxide cluster) and can be used to deposit the clusters on nearly any substrate without constraints of nucleation and growth [69].

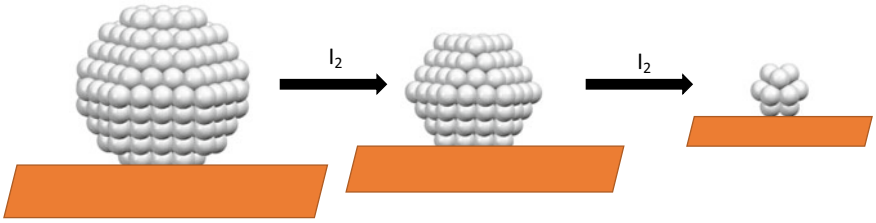

Fig. 1.7 Disaggregation of supported metal nanoparticles to clusters with iodine

Following top–down approaches (Fig. 1.7), redox active halogen species can be used to dislodge metal nanoparticles into sub-nanometer clusters. For instance, I_2 solutions broke Au NPs supported on charcoal, Al_2O_3, TiO_2 and ZnO, into sub-nanometric Au clusters and isolated atoms [50, 62, 63].

1.2.3 Metal Cluster Characterization Techniques

1.2.3.1 UV–Vis and Fluorescence

Ultraviolet-visible (UV–vis) spectrophotometric analysis is probably the easiest and fastest characterization method to determine the presence or absence of metal clusters in solution and also when supported on solids (diffuse reflectance mode). The appearance of absorption bands in the UV–A and blue visible regions (250–400 nm) can be indicative of the presence of metal clusters, which have defined valence orbitals, in clear contrast with metal nanoparticles which present plasmon bands in a different and non-interfering area, around 550 nm (Fig. 1.8). Based on the Jellium model presented above, the number of atoms of the clusters, N, can be calculated by the simple Eq. 1 ($E_F = 5.32$ eV for bulk Au) and Eg the HOMO–LUMO energy band gap, respectively (HOMO 1/4 highest occupied molecular orbital, LUMO 1/4

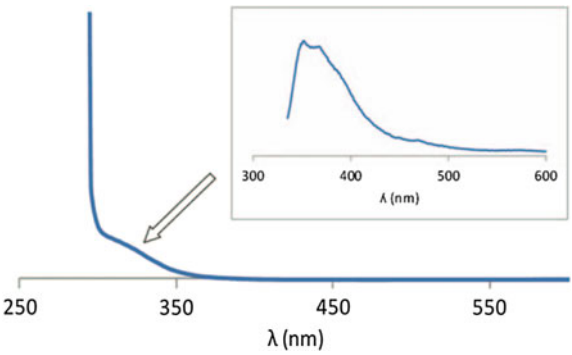

Fig. 1.8 Experimental absorption UV/Vis and the corresponding emission (inset) spectra for the AuIPrCl-catalyzed hydration of 1–octyne just after the induction time, where the formation of Au clusters (is completed) [53].

lowest unoccupied molecular orbital), which is obtained from the UV–vis spectrum. Thus, the absorption wavelength is directly correlated with atomicity and vice versa. Complementary emission (fluorescence) analysis circumvents the possible mask or interference by other absorbing species in UV–vis that could be present in the analyte, such as organic molecules and other metal compounds, since the clusters have the particularity of behaving as potent quantum dots. Thus, irradiation of the clusters in their corresponding absorbing wavelengths gives clear emission bands, which does not occur with most of organic compounds and metal precursors, including nanoparticles (see Fig. 1.8).

1.2.3.2 Mass Spectrometry

Routine and high-resolution electrospray ionization–mass spectrometry with quadrupole detectors are commonly employed to determine the empirical formula of metal clusters with ligands in solution, and matrix-assisted laser desorption/ionization time-of-flight (MALDI–TOF) spectrometers are used for solid samples. Following this, these mass spectrometry techniques can be employed not only to determine the mass of ligand-free metal clusters but also for selection, separation, isolation and deposition of individual clusters on solid surfaces [69]. Most metals show a unique isotopic pattern which unveils the atomicity of the cluster. Even for monoisotopic metals, such as the case of Au with a practical single isotope at 197 Da., mass spectrometry is useful since metal clusters appear beyond the minimum detectable mass of the instrumentation, typically 400 Da., which is a clear advantage with respect to lighter metals (Fig. 1.9) [55].

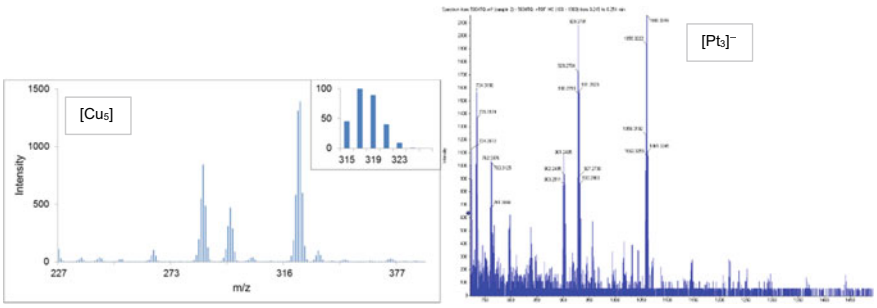

Fig. 1.9 Left: ESI–QTOF spectrum of small (Cu5) clusters in ethanol solution in negative ion mode with the simulation of the relative intensity peaks. Electrospray ionization/mass spectrometry with a quadrupole time-of-flight (ESI–QTOF) measurements of the samples. Right: ESI–QTOF measurements of Pt samples taken at 60 °C with 0.005 mol% of Karstedt's catalyst (reprinted with permission from Refs. [11 and 16]. Copyright © 2015 by American Chemical Society and Copyright © 2019 John Wiley & Sons, Inc., respectively)

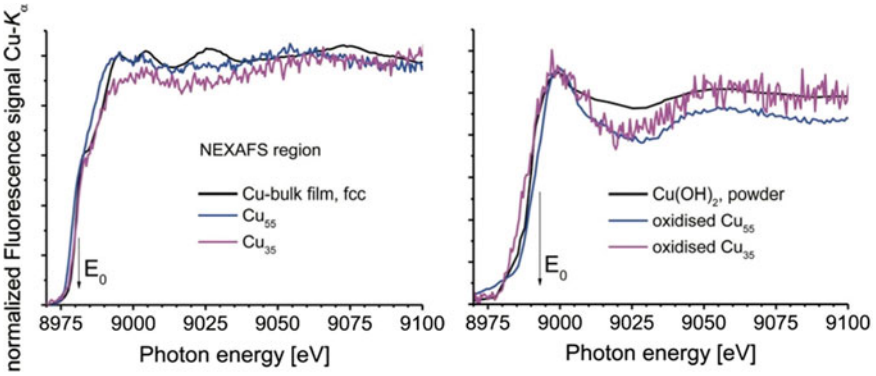

Fig. 1.10 NEXAFS region of the pristine (top) and oxidized (bottom) Cu_n clusters (n = 35, 55) in comparison with the respective bulk sample, Cu and $Cu(OH)_2$ (Fig. from [57]. Copyright © by The Royal Society of Chemistry 2016)

1.2.3.3 Synchrotron Techniques: EXAFS and XANES

Synchrotron techniques give information about the metal bonding and oxidation state and have been used for the determination of metal clusters on solids. However, determination of ligand-free metal clusters in solution with these techniques proved difficult since the highly diluted (typically micro- or nanomolar) conditions of the metal clusters are far below the detection limits of the instrumentation. For this reason, only few examples are available [57] (Fig. 1.10).

1.2.3.4 High Resolution Transmission Electron Microscopy (HR–TEM)

Transition metal elements are heavy, having very good response to the electron beam in EM techniques, particularly in unscattered, dark field mode. Thus, HR–TEM and high angle annular dark field–scanning transmission electron microscopy (HAADF–STEM) are routinely applied to the determination of supported metal nanoparticles and also clusters near or below the nanometer regime. For ultra-small metal clusters, aberration corrected HR–TEM must be employed. The solid support plays a role during visualization, and solids containing excessively heavy atoms or organic substances are more difficult to evaluate, since the former hide the metal atoms and the latter burn under the strong electron beam and spoil the microscopy detector. However, careful measurements have allowed the visualization of Au_5 clusters on carbon nanotubes and EVOH polymers. Indeed, HAADF–STEM has been employed to follow the evolution of supported Au atoms into Au clusters during reaction [10, 39] (Fig. 1.11).

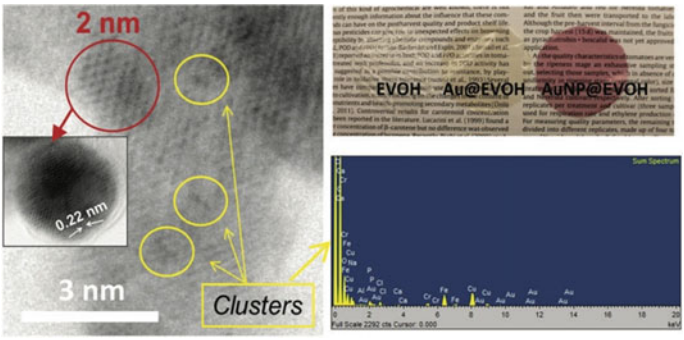

Fig. 1.11 Left: Aberration-corrected HR–TEM micrograph of Au@EVOH; the circles in yellow indicate Au clusters, the circle in red indicates a 2 nm Au NP, and the inset shows the interplanar crystallographic distance for Au. Top right: Photograph of neat EVOH (left, colorless), Au@EVOH (middle, yellow) and the material synthesized with carvacrol, which leads to plasmonic Au nanoparticles (right, red). Bottom right: A representative EDX spectrum of the area indicated for clusters, showing the presence of Au (Fig. from Ref. [50]. Copyright © by The Royal Society of Chemistry 2017)

1.2.3.5 Single Crystal X-Ray Diffraction

Perhaps, the more powerful technique for the structural determination of metal clusters is single crystal X-ray diffraction (SC–XRD). For ligand-stabilized clusters, this technique has been routinely employed, and for instance, the SC–XRD structure of a quasi-linear Pd_4 cluster stabilized and protected by polyarene ligands has been reported (Fig. 1.12) [47, 48]. However, this compound does not find application in catalysis since ligand exchange with the reactants triggers decomposition of the cluster even below 0 °C. In principle, decomposition may not occur in a ligand-free cluster suitably accommodated within a solid support, thus enabling heterogeneous catalysis by metal clusters. Indeed, the same quasi-linear Pd_4 cluster could be obtained in a robust and crystalline MOF structure with ability to incorporate and reduce metal cations [20]. The use of this type of MOFs has recently opened not only the possibility to prepare ligand-free few-atom sub-nanometer clusters but also to characterize them by SC–XRD and do catalysis with them. The MOF acts as a convenient crystalline matrix to host the ligand-free metal clusters and to obtain suitable monocrystals for diffraction, as it has been achieved not only for Pd but also for Pt clusters [45, 60].

1.2.3.6 Other Techniques

Dynamic light scattering (DLS) and zeta potential measurements

These techniques have been long employed to determine the size (DLS) and charge (zeta potential) of colloidal Au nanoparticles with the same instrumentation. Recent

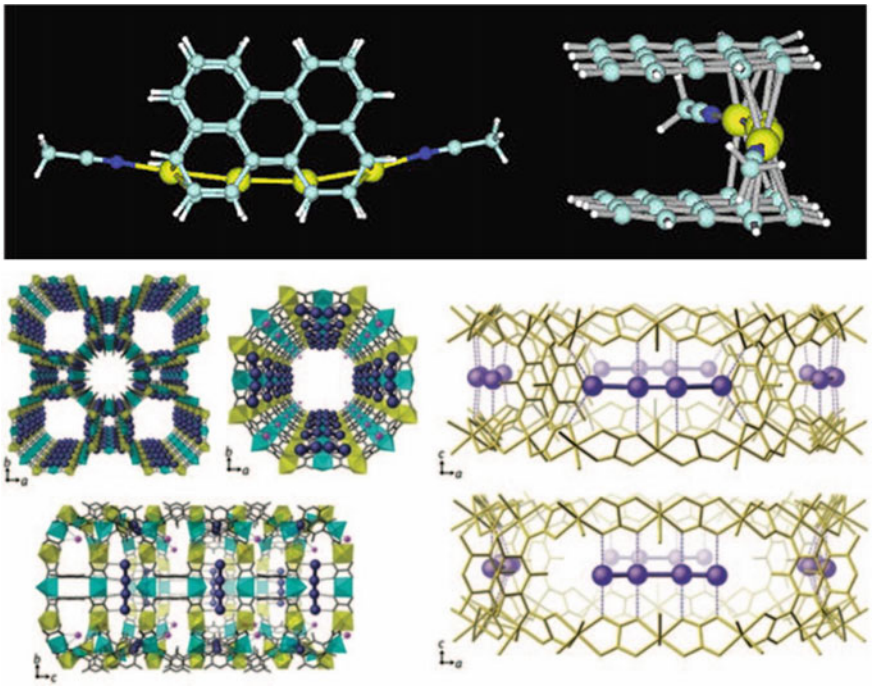

Fig. 1.12 Top: Single-crystal X-ray diffraction of a Pd_4 cluster stabilized by perylene ligands (Pd atoms are represented as yellow spheres) and within a MOF structure (Pd atoms are represented as purple spheres (Fig. extracted from Ref. [48]. Copyright © 2003 by American Chemical Society) Bottom: Perspective view along the b crystallographic axis of two portions (left) of the crystal structure of the MOF enclosing the two crystallographic not equivalent ligand-stabilized quasi-linear [Pd_4] clusters and DFT optimized structures (right). (Fig. adapted from Ref. [20] Copyright © 2017 by Nature Publishing Group)

advances of the technique allow the determination of the size and charge in soluble sub-nanometer metal clusters, down to a limiting resolution of 0.4 nm. Generally, polar solvents such as water, alcohols or amide solvents (*N, N*–dimethyl formamide, DMF, or *N*–methyl pyrrolidone, NMP) must be employed. Indeed, cationic $Au_{3–7}$, $Pd_{3–4}$ and $Pt_{3–5}$ clusters have been satisfactorily determined with this technique [17, 37, 49, 53]. The somehow related diffusion-ordered spectroscopy (DOSY) technique, which seeks to separate NMR signals of the clusters according to their diffusion coefficients, is also a valuable tool for organic-stabilized Au clusters but not for ligand-free metal clusters since a signal of the organic ligand must be monitored in the experiments [9, 21].

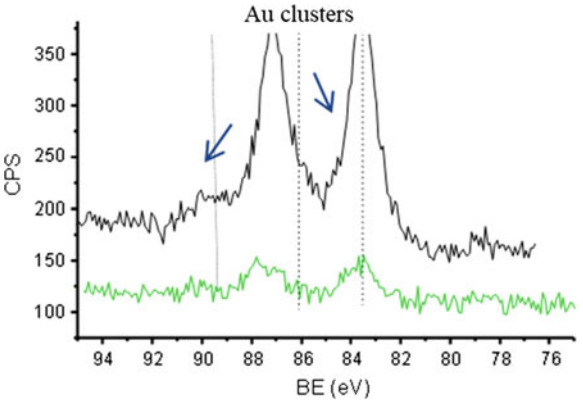

Fig. 1.13 XPS spectrum of a sample of Au–nCeO$_2$ after hydrogenation of 1 g of gold chloride on nanoceria at 200–300 °C under a flow of 100 ml per min of N_2:H_2 (10:1) (black line). The percentage of cationic Au in the reduced sample is 15% after deconvolution. For comparison, a sample of Au–nCeO$_2$ with a stronger reduction treatment—1 g of AuCl on ceria with 5 ml of phenylethanol at 160°C for 1 h (green line) —is also presented. The percentage of cationic Au decreases significantly to 2% (Fig. from Ref. [50]. Copyright © by The Royal Society of Chemistry 2017)

X-ray photoelectron spectroscopy (XPS)

XPS is a surface-sensitive and quantitative technique that allows one to determine the oxidation state of supported metal clusters. Either barely anchored to the solid surface or free in solution, metal clusters have been characterized with this technique, provided that the measurement is carried out with a relatively mild power in the X-ray beams, otherwise the metal clusters may further aggregate under operating conditions [50, 54]. Figure 1.13 shows a representative example of Au clusters.

Reaction test

The ester-assisted hydration of alkynes is a reaction exclusively catalyzed by Au clusters of 3–7 atoms ($Au_{3–7}$), and it has been developed as an analytical tool to unambiguously quantify sub-nanometer Au clusters and differentiate them from salts and nanoparticles (Fig. 1.14). For this, the reaction test was first validated with different samples of well-characterized sub-nanometer Au clusters on nanoceria (Au–nCeO$_2$) and then applied to a series of new solids containing sub-nanometer Au clusters [50]. This reaction test also allows for a very rapid quantification of the Au clusters in solution or on solids (after leaching them in situ under the test reaction conditions) without the requirements of any instrumental characterization but only a quantitative method to measure the evolution of the organic reaction, such as gas chromatography (GC) or nuclear magnetic resonance (NMR), using the initial rate of the reaction as a quantitative and linear parameter respect to the amount of $Au_{3–7}$ clusters in solution. (The reaction will be treated in detail in Sect. 1.3.2.1).

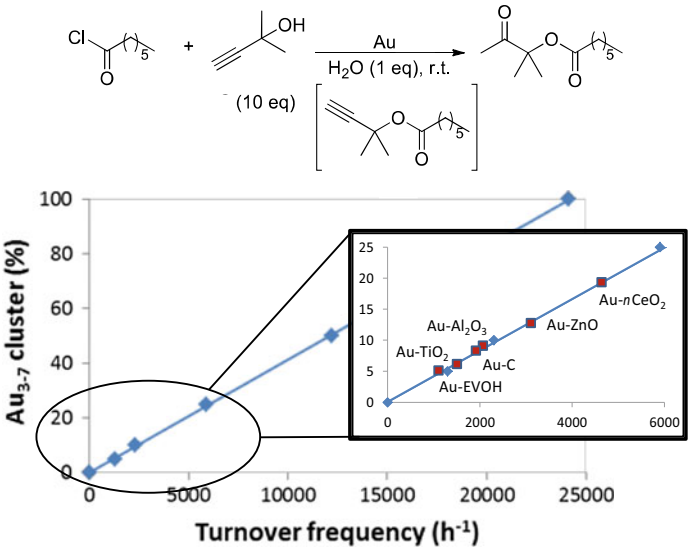

Fig. 1.14 Calibration line obtained for neat $Au_{3–7}$ clusters respect to their initial turnover frequencies and quantification of sub-nanometric Au clusters in the different Au-supported solids prepared here (inset), according to the test (Fig. from Ref. [50]. Copyright © by The Royal Society of Chemistry 2017)

1.3 Catalysis Using Metal Clusters

The most obvious benefit of a nanoscale catalyst is that it maximizes the surface area of the material and thereby increases the number of accessible sites for external reagents. For catalysis, exposing all metal atoms to outer reagents minimizes catalyst loading and save significant costs when using scarce noble metals (e.g., Au, Pd and Pt), which are nonetheless widely used in heterogeneous catalysis. With the development of modern methodologies to engineer the physical size, morphology and termination of nanoscale materials, the promise of exploiting the unique chemical properties of very small nanoparticles (< 5 nm) has now become feasible. No better example is the unique activity of small Au nanoparticles (< 2 nm), which are able to catalyze a wide range of oxidation reactions, whereas bulk Au is essentially inert, a singular property we are all familiar with in the macroscopic world [69]. Despite the unarguable success of nanocatalysis, recent advances in controlled atomic aggregation have stimulated enormous research interest for chemists to seek atomically precise particles; thus, cluster science is expected to bring a third upsurge of research interest due not only to the fascinating properties of clusters in solution but also to solid-supported clusters for catalysis. With the developments in instrumentation and technology, precise information regarding the breaking or formation of chemical bonds will become more clearly accessible. While the chemistry of solid-supported clusters and monolayer protected clusters (MPC) has become a topic of substantial

current interest, information on structural and electronic properties is often corroborated only by free gas-phase clusters. The stability of MPCs is often understood within the conceptual framework of superatoms validated in the gas phase on the basis of electronic shells.

In this respect, we summarize here the research advances in the catalytic activity of ligand-free metal clusters, either supported or not [14, 34, 38, 66, 70]. For that, we divide the reactions considering the new bond formed (carbon–carbon, carbon–heteroatom or heteroatom–heteroatom) and also in hydrogenation reactions. Oxidation reactions have been covered previously, and we do not discuss those here [29, 30].

1.3.1 Carbon–Carbon Bond–Forming Reactions

1.3.1.1 Heck, Suzuki and Sonogashira Couplings

Pd-catalyzed cross-coupling reactions are recognized as fundamental transformations in synthetic chemistry [71]. The general mechanism for these reactions (also under ligand-free conditions) involves an oxidative addition–reductive elimination cycle over a Pd(0) species generated in situ. Despite considerable effort during last three decades, the exact nature of the Pd^0 catalytic species remains a matter of debate [13]. It was recently found that $Pd_{3–4}$ clusters are formed from either Pd salts, complexes and nanoparticles in *N*–methylpyrrolidine (NMP) under heating conditions and are responsible for the catalytic activity during the Heck, Sonogashira, Stille and Suzuki coupling reactions of different iodo– and bromo–derivatives. The ligand-free $Pd_{3–4}$ clusters can be stored in aqueous solution to be used on demand and catalyze, for example, the Heck reaction under industrially viable conditions in high yields and with unprecedented turnover frequencies in some cases (Fig. 1.15). Despite this high activity, the activation of chloro–derivatives was not possible with this catalytic system, which highlights the still important role of ligands for particular molecule activations.

The use of metals in the form of sub-nanometer clusters can lead to a completely unexpected catalytic behavior for a given metal, and the Heck reaction is an illustrative example, recently uncovered [17]. As commented above, Pd clusters seem to be very active species for the Heck reaction which, however, is not surprising in terms of metal nature since Pd is the most common metal catalyst for this type of C–C coupling reaction. Indeed, the metal above Pd in the group X of the Periodic Table, Ni, is also active for this type of couplings but, in striking contrast, the metal below in the group X, Pt, is barely reported as a catalyst for C–C cross-coupling reactions. The lack of catalytic activity of Pt for these coupling reactions has been traditionally ascribed to the difficulties associated to single Pt atoms (in organometallic complexes) to efficiently shift between two electron oxidation states and thus promote the oxidative addition and the reductive elimination steps necessary to perform the coupling, without rapidly aggregating and losing activity. However, the

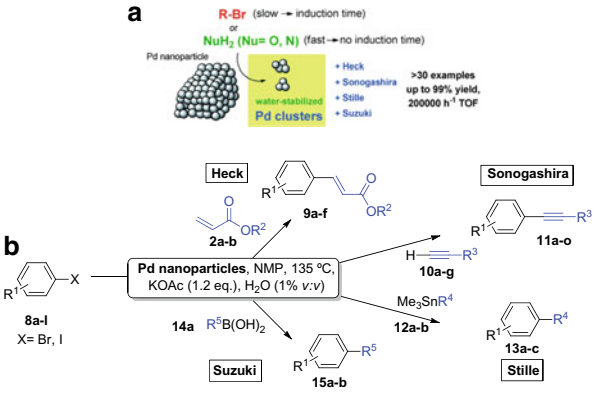

c

X	R^1	R^2/ R^3/ R^4/ R^5	Product	Pd (ppm)	TOF_0 [a]	Yield (%)[b]
I	*p*-COMe **8a**	R^2= *n*Bu **2a**	**9a**	3	$2.3 \cdot 10^5$	99
	H **8b**	R^2= *n*Bu **2a**	**9b**	30	$1.2 \cdot 10^4$	99
		R^3= *n*Oct **10a**	**11a**	300	$2.0 \cdot 10^3$	73
		R^3= Ph **10b**	**11b**	300	$7.2 \cdot 10^3$	83
		R^5= Ph **14a**	**15a**	30	$3.2 \cdot 10^3$	68
	p-Br **8c**	R^2= *n*Bu **2a**	**9c**	300	$3.6 \cdot 10^3$	99
		R^3= *n*Oct **10a**	**11c**	300	$3.1 \cdot 10^3$	99
	p-OMe **8d**	R^2= *n*Bu **2a**	**9d**	300	$3.2 \cdot 10^3$	99
		R^2= 2-Ethylhex **2b**	**9e**	3	$8.8 \cdot 10^4$	99
Br	*p*-COH **8e**	R^3= *n*Oct **10a**	**11d**	3	$2.0 \cdot 10^5$	99
		R^3= Ph **10b**	**11e**	300	$8.4 \cdot 10^3$	99
	o-COH **8f**	R^4= *n*Bu **12a**	**13a**	30	$8.2 \cdot 10^3$	91
	p-COMe **8g**	R^2= *n*Bu **2a**	**9a**	300	$3.1 \cdot 10^4$	99
		R^3= Ph **10b**	**11f**	300	$1.8 \cdot 10^4$	99
		R^3= *n*Oct **10a**	**11g**	300	$2.1 \cdot 10^3$	99
		R^3= *n*Oct **10a**	**11g**	0	-	<5
		R^4= *n*Bu **12a**	**13b**	3	$2.0 \cdot 10^5$	70[c]
		R^4= *n*Bu **12a**	**13b**	0	-	<5
		R^4= Ph **12b**	**13c**	3	$7.9 \cdot 10^4$	44
		R^5= Ph **14a**	**15b**	0.3	$1.0 \cdot 10^5$	61[c]
	H **8h**	R^2= *n*Bu **2a**	**9b**	300	$8.8 \cdot 10^2$	64
		R^3= *n*Oct **10a**	**11a**	300	$5.2 \cdot 10^3$	99
		R^3= *m*-tol **10c**	**11h**	300	$6.6 \cdot 10^3$	99
		R^3= *o*-tol **10d**	**11i**	300	$1.2 \cdot 10^3$	96
		R^3= *p*-anisole **10e**	**11j**	300	$2.4 \cdot 10^3$	99
		R^3= *o*-anisole **10f**	**11k**	300	$2.0 \cdot 10^3$	94
		R^3= *n*Dodec **10g**	**11l**	300	$8.0 \cdot 10^2$	97
		R^5= Ph **14a**	**15a**	30	$7.6 \cdot 10^3$	87
		R^5= Ph **14a**	**15a**	0	-	<5
	p-Me **8i**	R^3= *n*Oct **10a**	**11m**	300	$2.0 \cdot 10^3$	83
	o,p-OMe-Napth **8j**	R^3= *n*Oct **10a**	**11n**	300	$4.9 \cdot 10^3$	99
	o,o,p-Isoprop **8k**	R^2= 2-Ethylhex **2b**	**9f**	300	$1.1 \cdot 10^4$	35[c]
	p-OMe **8l**	R^2= *n*Bu **2a**	**9d**	300	$4.7 \cdot 10^2$	40
		R^2= *n*Bu **2a**	**9d**	0	-	<5
		R^3= Ph **10b**	**11j**	300	$2.8 \cdot 10^2$	50

Fig. 1.15 Reaction scheme for C–C coupling reactions catalyzed by Pd clusters formed in situ and catalytic results **a** TOF_0 is calculated on the basis of total amount of palladium and indicated as h^{-1}. **b** Product yields after 24 h. **c** Reaction temperature: 160 °C (Fig. from Ref. [5]. Copyright © 2014 by John Wiley & Sons, Inc.)

recent finding that Pt single atoms and clusters can be formed in solution has enabled the Pt-catalyzed Heck reaction of iodo– and bromo–derivatives [17]. Experimental studies in combination with DFT calculations strongly support the feasibility of the coupling mechanism steps on the Pt atoms, thus representing one example where the formation of ligand-free metal clusters unveils a somehow hidden catalytic behavior for a particular metal.

Recent theoretical studies on the electronic properties and activation energies for the three steps of the Suzuki cross-coupling reaction have shown that Pd/Ni bimetallic clusters supported on defected graphene can be excellent catalysts [72]. In fact, reducing the size of the clusters from Ni_{13} to Ni_4 enhances the activity because of the increased negative charge Pd. Bimetallic Pd/Ni clusters were found to offer even lower activation energies for all three steps of the Suzuki reaction because of charge donation from the Ni atoms to the Pd atoms making the bimetallic clusters a highly active catalyst.

1.3.1.2 Buchner Reaction

The ring-opening cyclopropanation of benzenes with alpha-diazoesters (Fig. 1.16) is known as the Buchner reaction. This reaction, despite its uniqueness to form otherwise very difficult to prepare cycloheptatrienes, giving access to a plethora of advanced organic intermediates, has found little use in industrial organic synthesis since the only efficient catalysts for the transformation are based on extremely expensive, soluble and unrecoverable Rh_2 salts [1].

Mixed-valence Pd_4 (0, I) clusters supported within a MOF have shown a high catalytic activity and selectivity, comparable to Rh_2 salts, for the Buchner reaction, enabling the performance of the reaction in continuous flow. The Pd_4 clusters have the appropriate electron density to activate the diazo-compound and generate the required carbene to open the benzene derivative. It is possible that, in line with

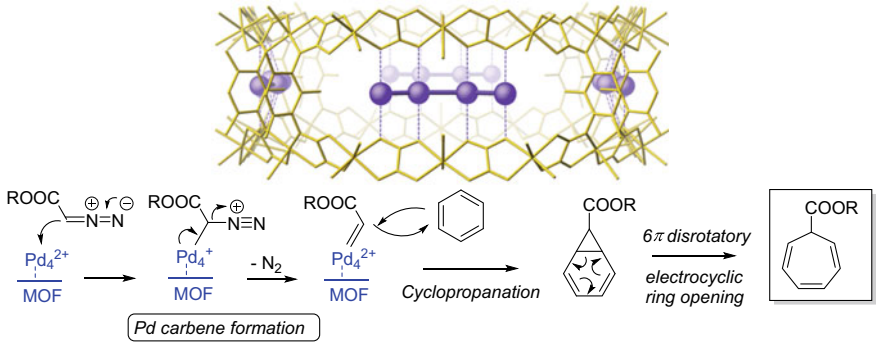

Fig. 1.16 Top: Pd_4 Cluster structure optimized by DFT calculations, on the basis of the real SC–XRD structure. Bottom: Proposed mechanism for the Pd4-catalyzed intermolecular Buchner reaction (Fig. from Ref. [20]. Copyright © 2017 by Nature Publishing Group)

the easy coordination of arene derivatives to this particular type of quasi-linear Pd_4 cluster, [46] the benzene molecule is also activated by the Pd_4 cluster to promote the final coupling. This recoverable Pd_4–MOF solid catalyst, with an estimated price 10–100 times lower than the Rh catalysts, constitutes a paradigmatic shift in the Buchner reaction, opening new avenues in the use of this reaction at larger scales under flow conditions.

1.3.1.3 Homocoupling of Alkynes

The homocoupling of alkynes is a classical organic reaction performed during years with Cu salts, in the Glaser, [24] Eglinton, [15] or Hay [27] versions. However, no significant reports on the use of the other two group XI metals, Ag and Au, as catalysts for the reaction have been shown, despite the electronic resemblance of these metals. When one examines the different accepted mechanisms for the Cu-catalyzed homocoupling of alkynes, it can be seen that a key step during the coupling is the oxidation of Cu(I) to Cu(III), a step intrinsically difficult for Ag but not so much for Au. Indeed, a second key feature during the homocoupling reaction is the plausible dimerization of the Cu atoms through coordinated alkyne bounds. Following this mechanistic rationale, it has been recently found that mixed-valence Au(I, III) clusters with ligands are very active species for the homocoupling of alkynes [36]. The particular structure of the cluster sterically discriminates between linear carbon chain alkynes with 10 or 12 atoms during the oxidative homocoupling of alkynes: the former is fully reactive, and the latter is practically unreactive. A distal size selectivity occurs by the impossibility of trans-metalating two long alkyl chains in an A-framed, mixed-valence di–Au (I, III) acetylide complex, as shown in Fig. 1.17. The reductive elimination of two alkyne molecules from a single Au(III) atom occurs extremely fast, in < 1 min at $-78°$ C (turnover frequency 40.016 s^{-1}). Notice that the extremely high catalytic activity of Au(III) and the stability of mixed Au(I, III) clusters for the homocoupling of alkynes is somewhat related to the relativistic effects present in the gold because is a lateheavy metal and absent in Cu and Ag [35]. The subtle steric and electronic discrimination of alkynes by this Au-catalyzed system allows the heterocoupling of two different alkynes in equimolecular amounts regardless of the nature of the terminal triple bond (Fig. 1.17).

It is not necessary to ligate the Au atoms through ligands to promote the homocoupling of alkynes since very small Au nanoparticles catalyze the aerobic coupling of alkynes [5]. For the latter, O_2 is dissociated as catalyzed by the air-tolerant Au nanoparticles, without significant oxidation of the metal. In contrast, ligand-free soluble sub-nanometer metal clusters do not dissociate O_2 in the presence of the alkyne and, thus, do not catalyze the aerobic coupling, [6] which makes sense considering the higher affinity of cationic Au atoms for alkynes than for O_2. These results exemplify the dramatic catalytic differences that can be found for a given metal in different aggregation forms, in this case Au, and when different ligands and supports are employed.

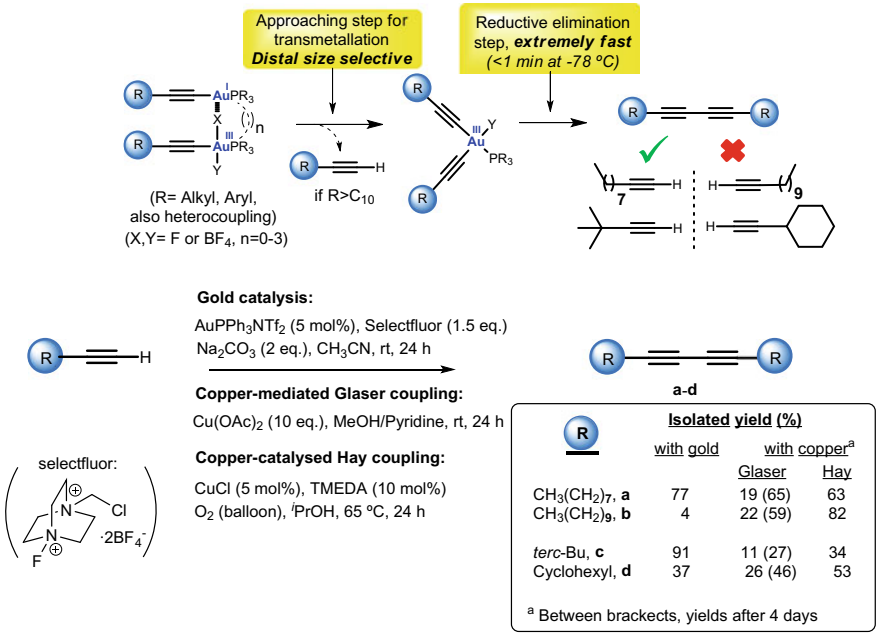

Fig. 1.17 Schematic mechanism of the Au-catalyzed oxidative homocoupling of terminal alkynes in solution. Notice the different reactivity of alkynes a–d found under the Au-catalyzed conditions reported here and typical copper-catalyzed conditions (Glaser or Hay conditions). Isolated yields are the average of two runs (Fig. from Ref. [36]. Copyright © 2015 by Nature Publishing Group)

1.3.1.4 Hashmi Phenol Synthesis

The rearrangement of alkynylfurans to prepare phenol derivatives has been reported by Hashmi et al. using Au salts and complexes [26]. Upon performing the reaction under conditions similar to those reported albeit with a lower amount of $AuCl_3$ (0.4 mol%), the corresponding product was smoothly formed after an induction time, as evidenced by ^1H NMR spectroscopy at different times (Fig. 1.18) [53]. MALDI–TOF measurements showed that the reaction started only after the formation of Au clusters comprising 3–4 atoms. These Au clusters can be formed also starting from AuCl and also from supported Au clusters on CeO_2 or leached from Au nanoparticles on TiO_2, with the assistance of a Brönsted acid.

1.3.1.5 Conia–ene Reaction

The Conia–ene reaction is an early example of Au-catalyzed carbon–carbon bond formation. In a pioneering work, Toste et al. showed that the Au(I) complex $AuPPh_3OTf$ (3 mol%) catalyzes the intramolecular coupling of electron-deficient

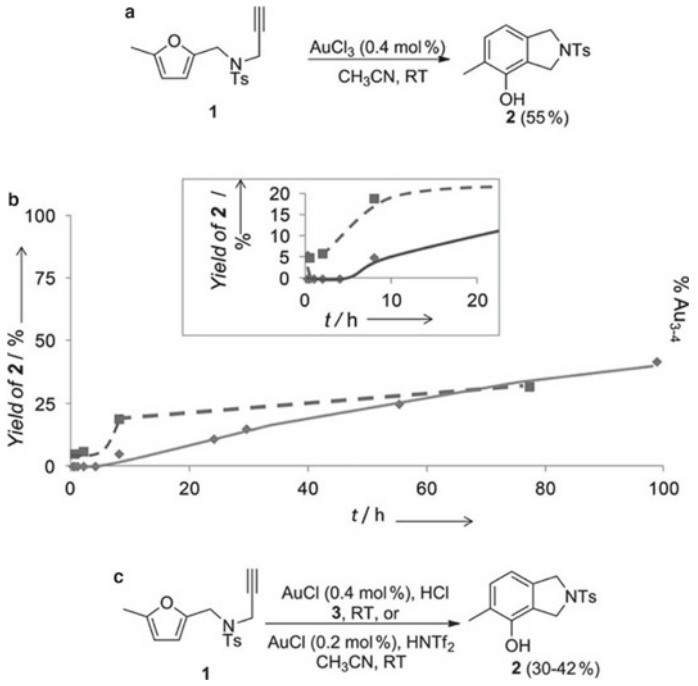

Fig. 1.18 **a** Phenol synthesis catalyzed by $AuCl_3$ (0.4 mol%). **b** Yield time plot for the phenol synthesis showed in scheme A above (**c**) and percentage of 3–4 atom Au clusters in solution according to MALDI–TOF MS measurements (**a**). The inset shows a magnification of the induction period when clusters formed. **c** Scheme for phenol synthesis by using AuCl as a catalyst in submolar amounts under two different reaction conditions (Fig. from Ref. [53]. Copyright © 2013 by John Wiley & Sons, Inc.)

α carbons to carbonyl groups with alkynes, whereas $AuCl_3$ was a very unselective catalyst, and only 30% of the cyclopentane product was obtained with a higher loading (10 mol%) of the Au salt after complete conversion [33]. Upon lowering the amount of AuCl and $AuCl_3$ to 0.02 mol%, no conversion was observed (Fig. 1.19) [53], but under acidic conditions (0.2 mol% of HOTf), the corresponding $Au_{3–6}$ clusters are formed to catalyze the reaction with similar results as $AuPPh_3OTf$.

1.3.2 Carbon–Heteroatom Bond-Forming Reactions

1.3.2.1 (Ester-Assisted) Hydration of Alkynes (C–O)

This reaction is the first example of catalysis by Au clusters formed in solution, as far as we know [49]. It can also be employed as a catalytic test to prove the presence of $Au_{3–5}$ clusters since the reaction only proceeds when the Au clusters are present in

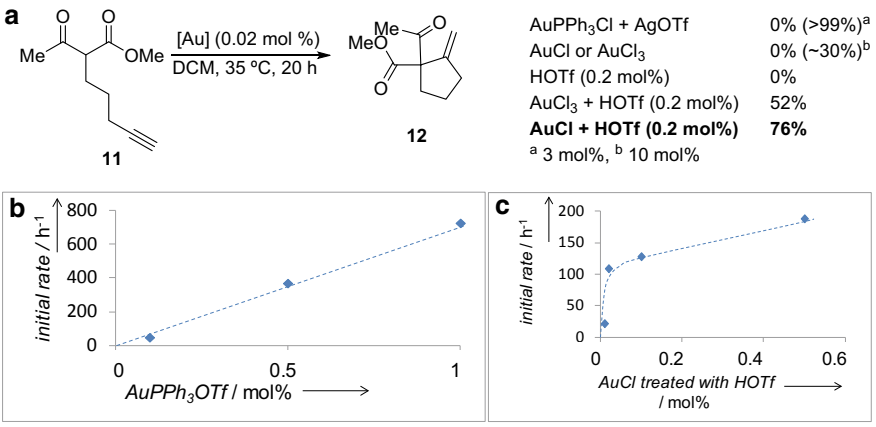

Fig. 1.19 **a** Results of the Au-catalyzed Conia–ene reaction of alkyne with different Au catalysts. **b** Initial rate dependence on the concentration of the initial $AuPPh_3OTf$ complex catalyst. **c** Initial rate dependence on the concentration of initial AuCl treated with HOTf. Lines are a guide for the eye (Fig. from Ref. [53]. Copyright © 2013 by John Wiley & Sons, Inc.)

the reaction media, even starting from part per billion amounts of Au salts, yielding a TON value as high as ~10^7 in some cases (Fig. 1.20). Notice that this value was substantially greater than any value reported for a non-enzymatic catalyst at room temperature at that time [4].

A systematic study of the cluster formation in different solvents and acids revealed that a variety of very small Au clusters, from 3 to 10 atoms, were formed under reaction conditions, with a size distribution controlled by the nature of both the solvent and the acid, as determined by UV–vis spectroscopy and mass spectrometry. However, Au_5 and Au_8 clusters stabilized on the dendrimer polyamineamide–ethanol, (PAMAM–OH) were synthesized independently and used as a catalyst, and the results showed that Au_5–PAMAM did indeed catalyze the ester-assisted hydration of alkynes, whereas Au_8–PAMAM showed a much lower activity, with no induction time in both cases. These results confirm the sensitivity of the reaction to the number of Au atoms in the cluster, showcasing perhaps one of the first examples of this class. It must be noted that the catalytic efficiency of the Au clusters when supported on the dendrimer was at least two orders of magnitude lower than that of those formed in situ in the propargyl alcohol, reflecting the inhibiting effect of ligands during the catalysis with few-atom soluble clusters.

1.3.2.2 Bromination of Aromatics and Alkynes (C–Br)

Together with the ester-assisted hydration of alkynes, the bromination of aromatics was one of the first examples of catalysis by Au clusters (Fig. 1.21) [49]. In this case, the formation of Au_7–Au_9 clusters occurred in the presence of the solvent

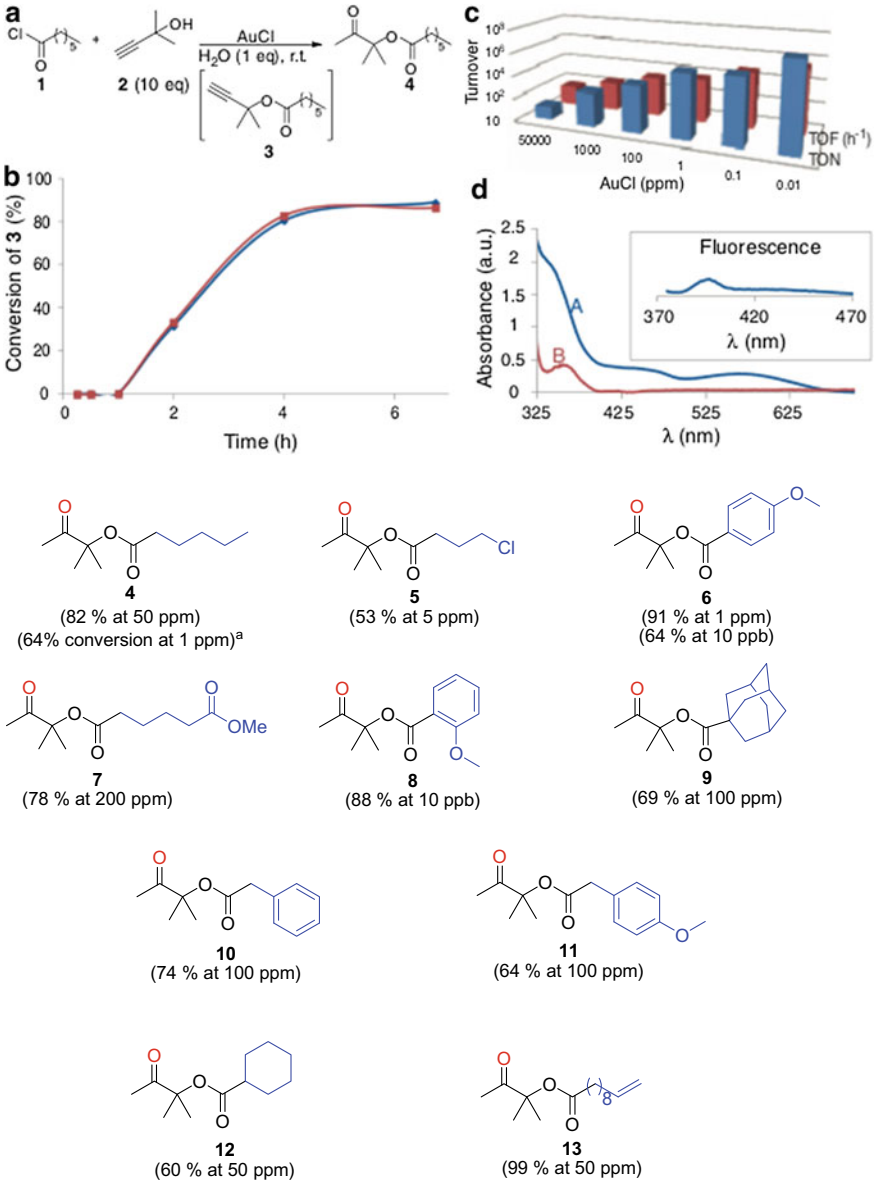

Fig. 1.20 **a** Ester-assisted hydration of in situ formed alkyne reaction. **b** Plot time conversion for AuCl (squares) and $HAuCl_4$ (diamonds) at 100 ppm, after correction with the blank experiment. **c** Turnover number (TON) and turnover frequency (TOF) for different amounts of AuCl, calculated as moles of 4 formed per mole of AuCl at final conversion (TON) and as the initial reaction rate after the induction time per mole of AuCl (TOF). The final yield of 4 is > 90% in all cases, except for 0.01 ppm, where it is ~ 50%. **d** Absorption measurements (a.u., arbitrary units) for the hydration of 3 containing the Au active species along the induction time (a) and when the reaction proceeds (b) with the corresponding fluorescence (inset, irradiated at 349 nm). Bottom, reaction scope (isolated yields and ppm of Au in parentheses (Fig. from Ref. [49]. Copyright © 2012 by AAAS)

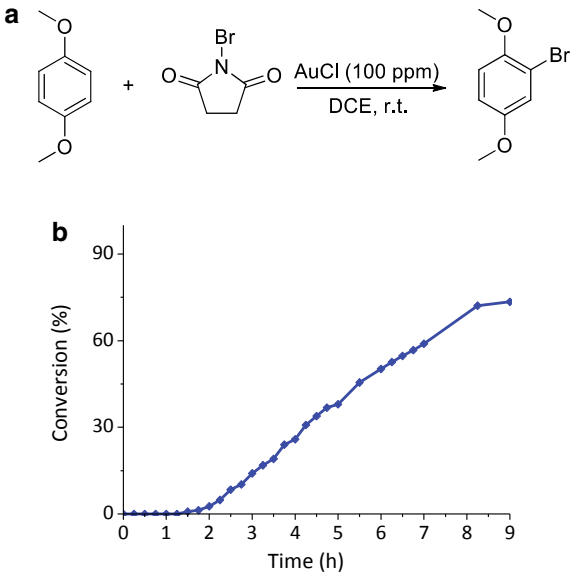

Fig. 1.21 **a** Studied reaction scheme. **b** Plot time conversion for the bromination of arene (Fig adapted from Ref. [49]. Copyright © 2012 by AAAS)

1,2–dichloroethane (DCE). In contrast to the ester-assisted hydration of alkynes, the reaction performed with Au_5–PAMAM and Au_8–PAMAM showed higher activity for the latter ones, in line with the $Au_{7\text{-}9}$ free clusters.

The ω-bromination of terminal alkynes catalyzed by Au complexes in solution is also a good example for C–Br bond formation catalyzed by Au clusters. Figure 1.22 shows that upon performing the reaction in the presence of $AuPtBu_3NTf_2$ (Tf = trifluoromethanesulfonyl) and by systematically decreasing the amount of Au from 2 to 0.1 mol%, a reaction induction time appeared [53]. Excellent yields of the bromated compound were obtained in all cases. Monitoring the reaction by ^{31}P NMR spectroscopy showed the progressive degradation of the Au complex during the reaction, whereas ^{19}F NMR spectroscopy showed the concomitant formation of free triflimidic acid ($HNTf_2$). According to these spectroscopic measurements, the degradation of $AuPtBu_3NTf_2$ provides the two elements needed for the formation and stabilization of the Au clusters: ligand-free Au species and a strong Brönsted acid.

Figure 1.23 shows that Au clusters are also formed from colloidal Au nanoparticles (10 ± 2.5) nm solution in HCl media and ω-bromination of phenylacetylene. Thus, this reaction illustrates how bottom–up (from Au salts) and top–down (from Au nanoparticles) synthetic approaches to metal clusters can equally work for a particular reaction. Given that a mixture of Au clusters from 3 to 10 atoms was formed in situ during reaction, it could be possible to carry out at the same time reactions catalyzed by different clusters. Indeed, an excess of *N*–bromosuccinimide (NBS) together with water present in the reaction medium allowed the one-pot Au-catalyzed hydration of a bromoalkyne to give α,α,'–dibromoketone in a single step in reasonable yield

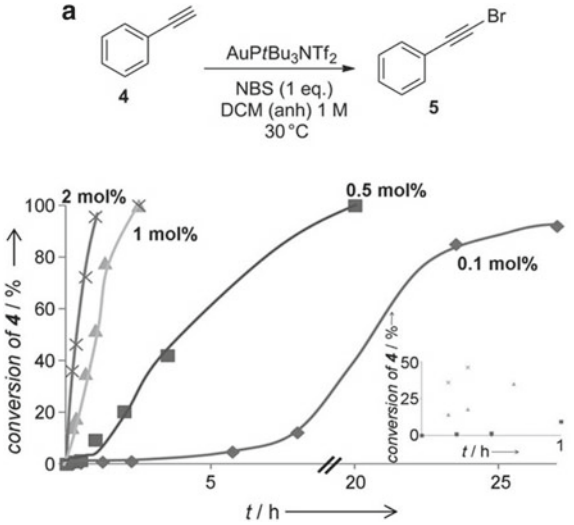

Fig. 1.22 Conversion time plot for the ω–bromination of phenylacetylene [4] with different amounts of the Au(I) $AuPtBu_3NTf_2$ complex catalyst. The inset maximizes the initial time (Fig. from Ref. [53]. Copyright © 2013 by John Wiley & Sons, Inc.)

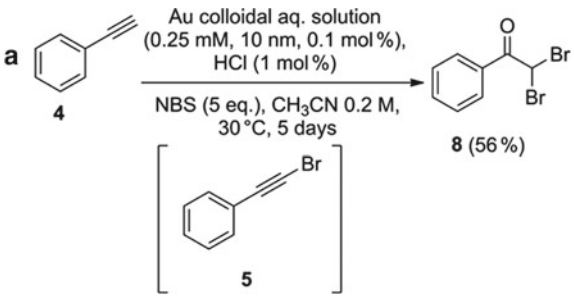

Fig. 1.23 **a** Bromination–hydration cascade with (10 ± 2.5) nm Au colloidal aqueous solution (0.25 mm, 0.1 mol%) treated with concentrated HCl (1 mol%, Fig. from Ref. [53]. Copyright © 2013 by John Wiley & Sons, Inc.)

after two consecutive Au-catalyzed reactions, one involving σ C–H activation and the other involving π activation of the alkyne.

1.3.2.3 Hydrosilylation of Alkynes (C–Si)

The hydrosilylation of alkynes gives three different possible vinylsilanes depending on the catalyst used (Fig. 1.24). Extensive research has been performed to obtain and functionalize the β-products (anti-Markovnikov addition), which can be formed

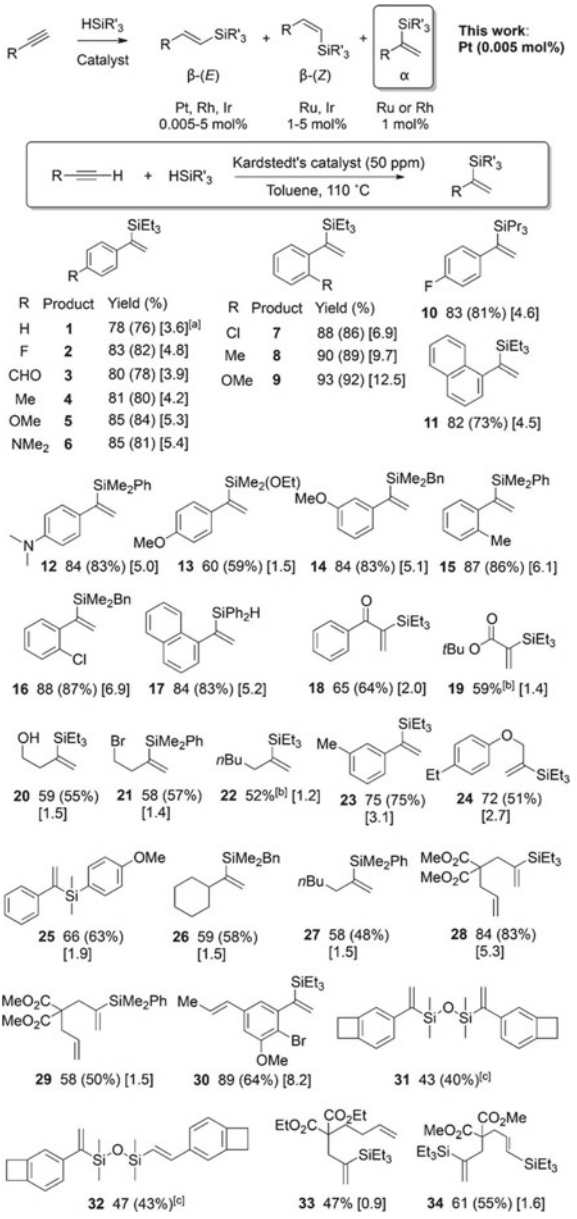

Fig. 1.24 Possible products in the hydrosilylation of terminal alkynes (top) and reaction scope for the Pt_3 clusters-catalyzed α– hydrosilylation: 0.005 mol% (50 ppm) of Kardstedt's catalyst (with respect to the alkyne) at 110 °C in toluene (0.5 M), GC yields, isolated yields of α isomer between parenthesis, and α/β ratio of the mixture, before isolation and calculated by GC–MS and ^{1}H NMR, between brackets, **a** 5–gram scale, **b** NMR yield, **c** Ratio $(\alpha\alpha)/(\alpha\beta)/(\beta\beta) = 43/47/10$ (bottom, Fig. adapted from Ref. [59]. Copyright © 2017 by John Wiley & Sons, Inc.)

in high yield and selectivity with ppm amounts of Pt catalyst or with other metal catalysts including Rh and Ir for the β–(*E*) product (the most thermodynamically stable) and Ru and Ir for the β–(Z)–vinylsilane. In order to get the α-vinylsilane, Pt_3 clusters were made to catalyze the Markovnikov hydrosilylation of terminal alkynes to afford a wide variety of new α-vinylsilanes in good isolated yields using low amounts of catalyst [59]. These clusters can be formed in situ with < 100 ppm of simple Pt compounds or with externally added Pt "Chini" clusters [41].

In order to prove that the Pt clusters were the active catalysts and not the precursors, UV–Vis absorption spectroscopy measurements were performed during reaction at 110 °C, in which the α-isomer is formed. These measurements showed the appearance of new bands at approximately 300 nm, and the fluorescence spectrum confirmed the expected emission band for $Pt_{3–4}$ (ca. 360 nm according to the Jellium model) when the α product was predominant. In contrast, only the plasmonic band of Pt nanoparticles was observed under β-favored reaction conditions, that is, reaction temperatures <70° C, without any absorption or emission band corresponding to sub-nanometer clusters. These results supported the formation of $Pt_{3–4}$ clusters during the hydrosilylation reaction at 110 °C with 0.005 mol% of Kardstedt's catalyst, without nanoparticle formation, and indicate that Pt clusters are the species needed for the α isomer formation. These results were confirmed also by Electro-Spray–Ionization Quadrupole Time-Of-Flight Mass Spectrometry (ESI–QTOF) and zeta potential measurements. Moreover, the Chini clusters [8] $[NEt_4]_2[Pt_3(CO)_6]_3$, $Na_2[Pt_3(CO)_6]_5$ and $Na_2[Pt_3(CO)_6]_{10}$ showed the production of α-vinylsilanes under classical (anti-Markovnikov) reaction conditions. The absence of induction time at the beginning in the reaction and the presence of the Pt_3 UV–VIS signals during the reaction confirmed that the Pt_3 clusters are the active catalysts for obtaining the α-isomer.

Considering the reactivity trends of the Pt_3 clusters, we can discuss the origin of the inverse selectivity toward the hydrosilylation with respect to the traditional Pt compounds. The Chalk–Harrod and a modified Chalk–Harrod mechanism are presented in Fig. 1.25, which is the most accepted mechanism for hydrosilylation of alkynes and alkenes catalyzed by Pt [42, 64]. Once the active catalyst is formed, the mechanism consists of four steps: (1) alkyne coordination to the Pt; (2) silane oxidative addition; (3) migratory insertion in Chalk–Harrod and silylplatination for modified Chalk–Harrod and (4) reductive elimination. Based on this mechanism, the key step that determines the regioselectivity of the reaction is the migratory insertion, which proceeds through hydroplatination for the former and silylplatination for the latter mechanism.

1.3.2.4 Andrussow Reaction (Cyanide Synthesis, C–N)

Hydrocyanic acid HCN is a very versatile molecule produced in multi-ton amounts using the Andrussow process. This process consists of an endothermic reaction between methane (CH_4) or carbon monoxide (CO) with ammonia (NH_3) at temperatures higher than 500 °C using Pt–Rh *gauze* catalysts in flow conditions to obtain

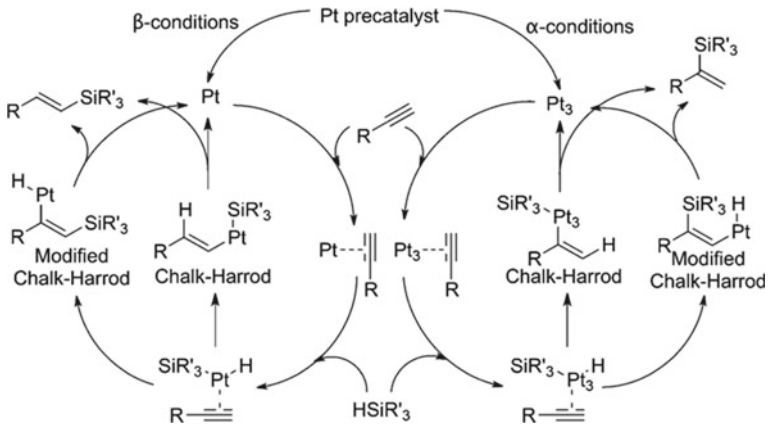

Fig. 1.25 Possible pathways for the hydrosilylation of alkynes to obtain β– (left) and α–alkenylsilanes (right) through both Chalk–Harrod and modified Chalk–Harrod mechanism (Fig. from Ref. [59]. Copyright © 2017 by John Wiley & Sons, Inc.)

hydrocyanic acid. Usually, the yields obtained for different Pt precursors are less than 10% with poor selectivity.

Pt_2^0 clusters homogeneously distributed and densely packed within the channels of a metal-organic framework were prepared (Fig. 1.26), unambiguously characterized by different techniques including SC–XRD, and employed as catalysts to perform the reaction of CO and NH_3 at nearly room temperature with a high TOF ($TOF_0 = 1260\ h^{-1}$). When monoatomic Pt^{2+} inside the same MOF was used as a catalyst, the TON decreased until 56. Moreover, no induction time was observed for Pt_2^0 clusters, confirming they are the active catalysts [45].

The reaction product was not the expected HCN but NH_4CN, a compound only stable below 40 °C but thermodynamically more accessible than HCN. Thus, the extremely high catalytic activity of the supported Pt_2^0 clusters do not only permit to activate CO and NH_3 at much lower temperature but also to bypass the reaction manifold to a more exothermic reaction, thus facilitating the gas conversion and shifting the chemical equilibrium to the right. These results with the hybrid material are significant from an economic and environmental viewpoint.

1.3.2.5 Goldberg Coupling (C–N)

The direct coupling of aryl halides with amides is known as the Goldberg coupling, and it has been recently found that sub-nanometer Cu clusters formed by endogenous reduction of Cu salts and Cu nanoparticles in heating amide solvents are active and selective catalysts for this C−N bond-forming reaction (Fig. 1.27). The Cu_{2-7} clusters were formed from different Cu salts to catalyze not only the Goldberg but also related C–P, C–O and even C–C couplings (Sonogashira reaction). Sub-nanometer

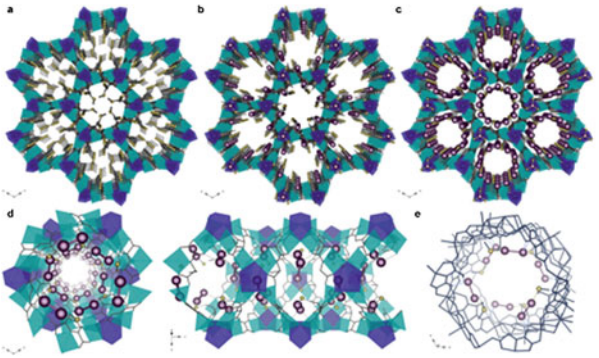

f

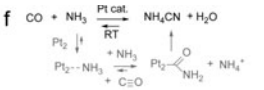

Entry	Catalyst	TON	TOF_0 (s^{-1})
1	–	–	–
2	$PtCl_4$	<1	–
3	$PtCl_2$	–	–
4	$Pt(acac)_2$	<1	–
5	PtO_2	–	–
6	$Na_2PtCl_6.xH_2O$	<1	–
7	$H_2PtCl_6.xH_2O$	–	–
8	$Pt(NH_3)_4(NO_3)_2$	–	–
9	$Pt(NH_3)_4(OH)_2$	–	–
10	$Pt(cod)Me_2$	–	–
11	$PtMe_3Cp$	–	–
12	$Pt(NH_3)_4Cl_2.xH_2O$	–	–
13	$Pt(PhCN)_2Cl_2$	–	–
14	$Pt(cod)Cl_2$	<1	–
15	Pt/C	–	–
16	Pt^{2+}/NaY	–	–
17	Pt/NaY	–	–
18	**1**	–	–
19	**2**	25	0.17
20	**3**	53	0.35

Fig. 1.26 Crystal structures of the MOF without metal (**a**, 1), with Pt_2^+ (**b**, 2) and with the Pt_2 clusters (**c**, 3). **d**. Perspective views, in detail, of a channel of 3 in the ab (left) and bc (right) planes. Copper and calcium atoms from the network are represented by cyan and blue polyhedra, respectively, whereas organic ligands are depicted as gray sticks. Yellow and purple spheres represent S and Pt atoms, respectively. Dashed lines represent the Pt···S interactions. **e**. Fragment of a channel of 3 emphasizing the interactions with the network. Pt–S and Pt…O interactions are represented by yellow and blue dashed lines, respectively. **f**. Pt-catalyzed synthesis of HCN at room temperature: Equation shows the reaction conditions: CO (4 bar, 1.5 mmol), NH_3 (2 bar, 0.75 mmol) and 0.0075 mmol Pt and a plausible reaction mechanism. Table includes the set of Pt catalysts tested under these reaction conditions (Fig. adapted from Ref. [45]. Copyright © 2018 by John Wiley & Sons, Inc.)

Cu clusters generated within a polymeric film show also activity for the C–N coupling and are a good example of metal cluster storage with full stability for months.

1.3.3 Heteroatom–Heteroatom Bond-Forming Reactions

1.3.3.1 Hydrosilylation of Alcohols

Alcohol hydrosilylated compounds are traditionally used as intermediates in organic synthesis. *O*–Silylation often competes so successfully with *C*–silylation that protective groups must be used to avoid *O*–silylation; however, only *O*–silylated compounds are formed for Pt catalysts used in low concentrations. Specifically for allyl alcohols, it was found that no *O*–silylation was obtained at 50 mM Pt catalyst concentration, and ~3 and 7% O–silylation occurred when [Pt] is 20 and 10 mM, respectively [75]. Furthermore, much more forcing conditions were required at the lower catalyst concentrations. These results suggest a change in the nature of the active catalyst species. Moreover, during the catalyst preparation, Pt_2 clusters were detected.

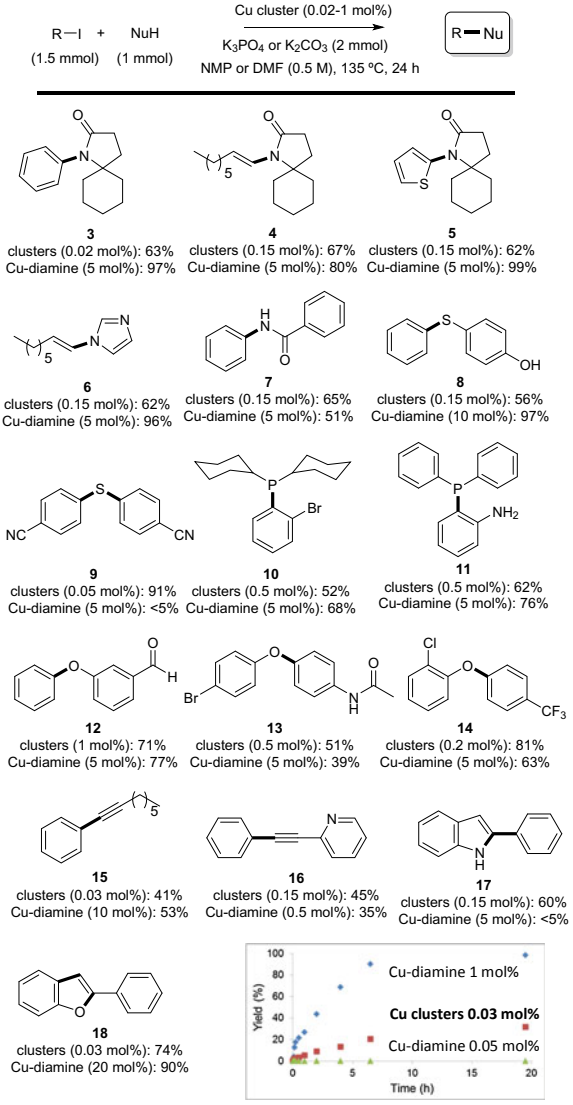

Fig. 1.27 Scope of the Cu cluster-catalyzed cross-coupling reactions. Isolated yields. The new bonds are in bold. For comparison, the values with Cu–diamine catalysts are also given, reaction conditions: substrates (1 mmol), CuI (5–20 mol%), N,N–methyl ethylenediamine (10–40 mol%), K_3PO_4 (2 mmol), anhydrous toluene or dioxane (0.25 M), nitrogen atmosphere, 110 °C, 24 h. The inset shows the kinetics for the Goldberg coupling between the iodobenzene and the amide under typical reaction conditions for diamine-assisted coupling and the conditions reported (Fig. from Ref. [54]. Copyright © 2015 by American Chemical Society)

1.3.3.2 Homocoupling of Thiols

The homocoupling of thiols is another clear example of catalysis by Au clusters. In this case, single Au atoms supported on functionalized carbon nanotubes only show activity in the oxidation of thiophenol with O_2 when they aggregate under reaction conditions into Au clusters of low atomicity (see induction period in Fig. 1.28) [5, 10]. The $Au_{5–10}$ are extremely active for the reaction, with TOFs in the order of 10^5 h^{-1}, comparable to the activity of sulfhydryl oxidase enzymes. When clusters grow into nanoparticles of diameter $\geq$1 nm, catalyst activity drops to zero. Theoretical calculations show that only Au clusters of low atomicity are able to simultaneously adsorb and activate thiophenol and O_2 and that the strong Au–S interaction in 1 nm Au nanoparticles leads to the formation of very stable RS–Au–SR units that prevent further reaction (Fig. 1.28 right). The combination of activation of both reactants and facile product desorption makes Au clusters excellent catalysts.

In turn, the aerobic thiol coupling is a reaction mechanistically similar to alkyne coupling, where H_2O is generated as a by-product after O_2 dissociation and coupling on the Au atoms, which, in principle, should not occur on Au nanoparticles since thiols are recurrently used as ligands to generate and stabilize Au nanoparticles [18, 76]. Thus, it is not surprising that the reaction only occurs on few-atom Au

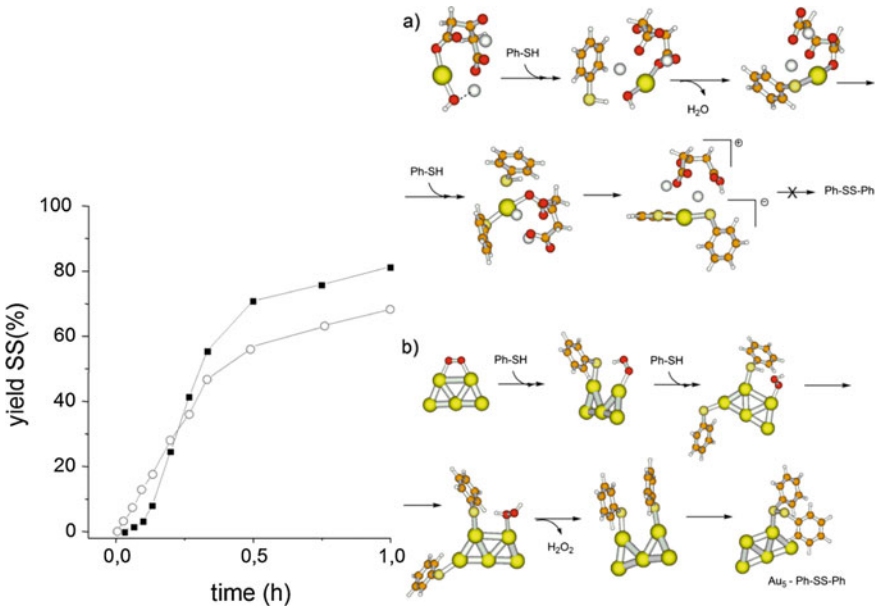

Fig. 1.28 Left: Yield to disulfide with reaction time over Au atoms (black squares) and over Au clusters (empty circles). Au nanoparticles are inactive. Right: Structures involved in the mechanism of thiol oxidation catalyzed by **a** AuI species and **b** Au_5 cluster. Au, S, C, O and H atoms are yellow, orange, red and white, respectively (Fig. adapted from Ref. [5]. Copyright © 2014 American Chemical Society)

clusters since, in contrast to alkynes, the strength of the coordination bond with thiols decreases as the Au particle decreases in size. The isolated Au atoms are not the true catalyst of the homocoupling but just precursors that evolve during reaction to few-atom Au clusters, which are indeed the catalytically active species (see Fig. 1.28).

1.3.4 Hydrogenation Reactions

The hydrogenation of unsaturated bonds is perhaps one of the older transformations with catalytic metals. Typically performed with finely divided metal powders and modernly with metal nanoparticles, the hydrogenation is widely accepted to proceed by H_2 dissociation and spillover of the H atoms on the metal and/or support surface. For this reason, the use of supported single metal atoms or clusters was not considered until recently. Indeed, it has been found that not only H_2 dissociation [40] but also H_2 formation [43] occurs very efficiently over supported isolated metal atoms and clusters [12, 19, 22, 74]. Two representative reaction examples for catalytic clusters follow, although much more can be found in the literature [28, 68].

1.3.4.1 CO_2 Methanation

The hydrogenation of CO_2 to methane (Sabatier reaction) is one of the oldest metal-catalyzed hydrogenation reactions, which is now revisited due to the urgent need of converting CO_2 to useful chemicals and, concomitantly, alleviating its global warming effect [23]. For that, it is convenient to design metal catalytic systems that operate at low temperatures (< 250 °C). It has been recently reported that Pt_2^0 clusters inside a MOF catalyze the reaction at temperatures below 150 °C, and comparison between isolated Pt atoms inside the same MOF and reference catalysts shows that the Pt cluster outperforms the rest of materials tested under the low-temperature conditions, including the industrial catalyst Ru–Al_2O_3 (Fig. 1.29) [45]. The lack of activity of Pt^{2+} discards these sites as catalytic active species and indicates that Pt_2^0 is the catalytic sites for the hydrogenation of CO_2.

1.3.4.2 Olefin Hydrogenation

Olefin hydrogenation is another typical example of a metal-catalyzed reaction with industrial application [73]. The Pt_2^0 clusters supported in the MOF also efficiently catalyze the hydrogenation of ethylene under industrial reaction conditions, in flow, at much lower temperature (60 °C) than current industrial processes with nanoparticles (200–400 °C) and with a sustained TOF of 250 h^{-1} (Fig. 1.30) [45]. Moreover, other < C_6 alkenes such as propylene, 1, 3–butadiene and 1–hexene, among others reacted similarly well. Also, when isomerically pure *E*–3–hexene was hydrogenated with

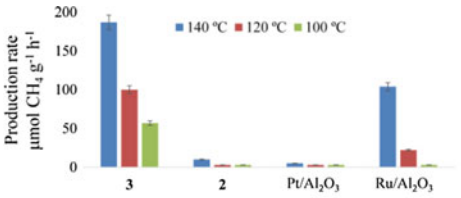

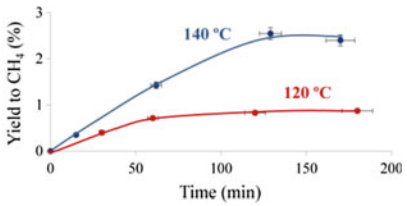

Catalyst[25]	Temperature (º C)	Reaction pressure (bar)	Activation energy (KJ mol^{-1})
Ni 58%	275–325	7–17	61
Ru/Al_2O_3 10wt%	200–300	1	66
Ru/Al_2O_3 0.5wt%	200–400	1	68
3	**100–140**	**4**	**35**

Fig. 1.29 Pt-catalyzed methanation of CO_2. Reaction conditions: 7 ml CO2 (1 atm, 0.28 mmol), 7 ml N_2 (internal standard, 1 atm, 0.28 mmol), 7 ml H2 (4 atm, 1.12 mmol), MOF catalyst with Pt_2^+ (**2**) and Pt_2^0 (**3**) (8 wt%, 20 mg, 0.008 mmol metal) or M/Al_2O_3 (5 wt%, 32 mg, 0.008 mmol metal), 100–140 °C, 6 h. Table includes reaction values for reference literature catalysts and catalyst **3** (Fig. adapted from Ref. [45]. Copyright © 2018 by John Wiley & Sons, Inc.)

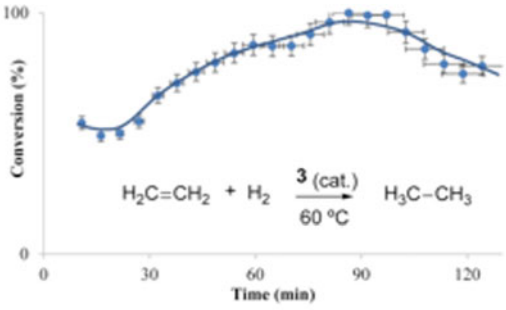

Catalyst	Temperature (º C)	Reaction pressure (bar)	Activation energy (KJ mol^{-1})
Pd/SiO_2	80–120	1	36
$Pd–Ag/SiO_2$	80–120	1	32
3	40–80	5	32

Fig. 1.30 Pt-catalyzed hydrogenation of ethylene: Equation shows the reaction conditions: 2 ml/min C_2H_4, 6 ml/min H_2, atmospheric pressure, 60 °C, 50 mg of Pt_2^0–MOF (**3**, 0.010 mmol Pt). Table includes reaction values for reference literature catalysts and catalyst **3** (Fig. adapted from Ref. [45]. Copyright © 2018 by John Wiley & Sons, Inc.)

Pt_2^0 as a catalyst, the corresponding isomerized intermediate *Z*–3–hexene was found during reaction, which supports a Langmuir–Hinshelwood type mechanism.

1.4 Conclusions

Ligand-free sub-nanometer metal clusters with a precise number of metal atoms are extremely active and selective catalysts for a variety of organic reactions which include carbon–carbon, carbon–heteroatom and heteroatom–heteroatom bond-forming reactions and hydrogenation reactions, among others.

The synthesis of the tiny metal clusters is simple and can be performed by bottom–up (from metal salts and complexes) and top–down (from nanoparticles) approaches. In solution, mild reducing agents such as amide solvents and alcohols or dislodging agents such as Brönsted acids (HCl, HOTf) are employed, but often, these external agents are not necessary, and the same organic reagents trigger and organize the formation of the catalytically active metal clusters during reaction, provided that the metal is sufficiently diluted to avoid further agglomeration. These soluble metal clusters can be stored either in amide or alcohol solutions or in solids (polymeric films, inorganic oxides) to be used on demand for different organic reactions. For the synthesis of the solid-supported, ligand-free sub-nanometer clusters, much stronger reducing agents, such as $NaBH_4$ or H_2, can be employed since the strong interaction between the sub-nanometer cluster and the support avoids further agglomeration. These solid supported clusters are generally more homogeneous in atomicity, spatial distribution and size than those formed in solution and do not require dilution with loadings up to 8 wt% in a MOF.

Modern characterization techniques, including SC–XRD and aberration-corrected TEM, have sufficient technological ability to determine the exact number of atoms, oxidation state and topological distribution of the metal cluster, in other words, a complete structural and electronic information. With this in hand, and also in combination with well-advanced theoretical calculations for cluster chemistry, researchers should now be able to predict the catalytic behavior for a given metal cluster in different reactions and ultimately design the metal cluster needed for a target (and perhaps new) reaction.

References

1. Anciaux AJ, Demonceau A, Noels AF et al (1981) Transition-metal-catalyzed reactions of diazo compounds. 2. Addition to aromatic molecules: catalysis of Buchner's synthesis of cycloheptatrienes. J Org Chem 46:873–876. https://doi.org/10.1021/jo00318a010
2. Bayram E, Linehan JC, Fulton JL et al (2011) Is It Homogeneous or Heterogeneous Catalysis Derived from [RhCp*Cl2]2? In Operando XAFS, Kinetic, and Crucial Kinetic Poisoning Evidence for Subnanometer Rh4 Cluster-Based Benzene Hydrogenation Catalysis. J Am Chem Soc 133:18889–18902. https://doi.org/10.1021/ja2073438
3. Bittner AM, Wu XC, Balci S, et al (2005) Bottom-up synthesis and top-down organisation of semiconductor and metal clusters on surfaces. Eur. J. Inorg. Chem. 3717–3728. https://doi.org/10.1002/ejic.200500388
4. Bogdanović B, Spliethoff B, Wilke G (1980) Dimerization of propylene with catalysts exhibiting activities like highly-active enzymes. Angew Chemie Int Ed English 19:622–623. https://doi.org/10.1002/anie.198006221

5. Boronat M, Laursen S, Leyva-Perez A et al (2014) Partially oxidized gold nanoparticles: a catalytic base-free system for the aerobic homocoupling of alkynes. J Catal 315:6–14. https://doi.org/10.1016/j.jcat.2014.04.003
6. Boronat M, Leyva-Perez A, Corma A (2014) Theoretical and experimental insights into the origin of the catalytic activity of subnanometric gold clusters: attempts to predict reactivity with clusters and nanoparticles of gold. Acc Chem Res 47:834–844. https://doi.org/10.1021/ar400068w
7. Buceta D, Busto N, Barone G et al (2015) Ag2 and Ag3 Clusters: synthesis, characterization, and interaction with DNA. Angew Chemie Int Ed 54:7612–7616. https://doi.org/10.1002/anie.201502917
8. Calabrese JC, Dahl LF, Chini P et al (1974) Synthesis and structural characterization of platinum carbonyl cluster dianions bis, tris, tetrakis, or pentakis(tri-μ2-carbonyl-tricarbonyltriplatinum)(2-). New series of inorganic oligomers. J Am Chem Soc 96:2614–2616. https://doi.org/10.1021/ja00815a050
9. Carenco S, Leyva-Perez A, Concepcion P et al (2012) Nickel phosphide nanocatalysts for the chemoselective hydrogenation of alkynes. Nano Today 7:21–28. https://doi.org/10.1016/j.nantod.2011.12.003
10. Corma A, Concepción P, Boronat M et al (2013) Exceptional oxidation activity with size-controlled supported gold clusters of low atomicity. Nat Chem 5:775
11. Daniel M-C, Astruc D (2004) Gold nanoparticles: assembly, supramolecular chemistry, quantum-size-related properties, and applications toward biology, catalysis, and nanotechnology. Chem Rev 104:293–346. https://doi.org/10.1021/cr030698+
12. Ding K, Gulec A, Johnson AM (2015) Identification of active sites in CO oxidation and water-gas shift over supported Pt catalysts. Science (80);350:189 LP–192. https://doi.org/10.1126/science.aac6368
13. Durand J, Teuma E, Gómez M (2008) An overview of palladium nanocatalysts: Surface and molecular reactivity. Eur. J. Inorg. Chem. 3577–3586. https://doi.org/10.1002/ejic.200800569
14. Dyson PJ (2004) Catalysis by low oxidation state transition metal (carbonyl) clusters. Coord Chem Rev 248:2443–2458. https://doi.org/10.1016/j.ccr.2004.04.002
15. Eglinton G, Galbraith AR (1959) 182. Macrocyclic acetylenic compounds. Part I. Cyclotetradeca-1 :3-diyne and related compounds. J. Chem. Soc. 889–896. https://doi.org/10.1039/jr9590000889
16. Faraday M (1857) Experimental relations of gold {and other Metals) to Light. B y. Philos Trans 147:145
17. Fernandez E, Rivero-Crespo MA, Dominguez I et al (2019) Base-controlled heck, suzuki, and sonogashira reactions catalyzed by ligand-free platinum or palladium single atom and sub-nanometer clusters. J Am Chem Soc 141:1928–1940. https://doi.org/10.1021/jacs.8b07884
18. Ferrando R, Jellinek J, Johnston RL (2008) Nanoalloys: from theory to applications of alloy clusters and nanoparticles. Chem Rev 108:845–910. https://doi.org/10.1021/cr040090g
19. Flytzani-Stephanopoulos M, Gates BC (2012) Atomically dispersed supported metal catalysts. Annu Rev Chem Biomol Eng 3:545–574. https://doi.org/10.1146/annurev-chembioeng-062011-080939
20. Fortea-Perez FR, Mon M, Ferrando-Soria J et al (2017) The MOF-driven synthesis of supported palladium clusters with catalytic activity for carbene-mediated chemistry. Nat Mater 16:760–766. https://doi.org/10.1038/nmat4910
21. Frogneux X, Pesesse A, Delacroix S et al (2019) Radical-initiated dismutation of hydrosiloxanes by catalytic potassium-graphite. ChemCatChem. https://doi.org/10.1002/cctc.201900172
22. Fu Q, Saltsburg H, Flytzani-Stephanopoulos M (2003) Active nonmetallic Au and Pt species on ceria-based water-gas shift catalysts. Science (80);301:935 LP–938. https://doi.org/10.1126/science.1085721
23. Ghaib K, Nitz K, Ben-Fares F-Z (2016) Chemical methanation of CO2: a review. Chem Bio Eng Rev 3:266–275. https://doi.org/10.1002/cben.201600022
24. Glaser C (1870) Untersuchungen über einige derivate der zimmtsäure. Justus Liebigs Ann Chem 154:137–171. https://doi.org/10.1002/jlac.18701540202

25. Grancha T, Ferrando-Soria J, Zhou H-C et al (2015) Postsynthetic improvement of the physical properties in a metal-organic framework through a single crystal to single crystal transmetalation. Angew Chemie, Int Ed 54:6521–6525. https://doi.org/10.1002/anie.201501691
26. Hashmi ASK, Frost TM, Bats JW (2000) Highly selective gold-catalyzed arene synthesis. J Am Chem Soc 122:11553–11554. https://doi.org/10.1021/ja005570d
27. Hay AS (1962) Oxidative coupling of acetylenes. ii1. J Org Chem 27:3320–3321. https://doi.org/10.1021/jo01056a511
28. Hernández E, Bertin V, Soto J et al (2018) Catalytic reduction of nitrous oxide by the low-symmetry pt8 cluster. J Phys Chem A 122:2209–2220. https://doi.org/10.1021/acs.jpca.7b11055
29. Herzing AA, Kiely CJ, Carley AF, et al (2008) Identification of active gold nanoclusters on iron oxide supports for CO oxidation. Science (80) 321:1331 LP–1335. https://doi.org/10.1126/science.1159639
30. Ikuno T, Zheng J, Vjunov A et al (2017) Methane oxidation to methanol catalyzed by cu-oxo clusters stabilized in nu-1000 metal-organic framework. J Am Chem Soc 139:10294–10301. https://doi.org/10.1021/jacs.7b02936
31. Imaoka T, Akanuma Y, Haruta N et al (2017) Platinum clusters with precise numbers of atoms for preparative-scale catalysis. Nat Commun 8:688. https://doi.org/10.1038/s41467-017-00800-4
32. Imaoka T, Yamamoto K (2019) Wet-chemical strategy for atom-precise metal cluster catalysts. Bull Chem Soc Jpn 92:941–948. https://doi.org/10.1246/bcsj.20190008
33. Kennedy-Smith JJ, Staben ST, Toste FD (2004) Gold(I)-catalyzed conia-ene reaction of β-ketoesters with alkynes. J Am Chem Soc 126:4526–4527. https://doi.org/10.1021/ja049487s
34. Leyva-Perez A (2017) Sub-nanometre metal clusters for catalytic carbon-carbon and carbon-heteroatom cross-coupling reactions. Dalt Trans 46:15987–15990. https://doi.org/10.1039/C7DT03203J
35. Leyva-Perez A, Corma A (2012) Similarities and differences between the "relativistic" triad gold, platinum, and mercury in catalysis. Angew Chemie, Int Ed 51:614–635. https://doi.org/10.1002/anie.201101726
36. Leyva-Perez A, Domenech-Carbo A, Corma A (2015) Unique distal size selectivity with a digold catalyst during alkyne homocoupling. Nat Commun 6:6703. https://doi.org/10.1038/ncomms7703
37. Leyva-Perez A, Oliver-Meseguer J, Rubio-Marques P, Corma A (2013) Water-stabilized three- and four-atom palladium clusters as highly active catalytic species in ligand-free C-C cross-coupling reactions. Angew Chemie, Int Ed 52:11554–11559. https://doi.org/10.1002/anie.201303188
38. Liu L, Corma A (2018) Metal catalysts for heterogeneous catalysis: from single atoms to nanoclusters and nanoparticles. Chem Rev (Washington, DC, United States) 118:4981–5079. https://doi.org/10.1021/acs.chemrev.7b00776
39. Liu L, Zakharov DN, Arenal R et al (2018) Evolution and stabilization of subnanometric metal species in confined space by in situ TEM. Nat Commun 9:1–10. https://doi.org/10.1038/s41467-018-03012-6
40. Liu P, Zhao Y, Qin R, et al (2016) Photochemical route for synthesizing atomically dispersed palladium catalysts. Science (80) 352:797 LP–800. https://doi.org/10.1126/science.aaf5251
41. Longoni G, Chini P (1976) Synthesis and chemical characterization of platinum carbonyl dianions [Pt3(CO)6]n2- (n = .apprx.10,6,5,4,3,2,1). A new series of inorganic oligomers. J Am Chem Soc 98:7225–7231. https://doi.org/10.1021/ja00439a020
42. Marciniec B (2008) Hydrosilylation of unsaturated carbon—heteroatom bonds
43. Marcinkowski MD, Liu J, Murphy CJ et al (2017) Selective formic acid dehydrogenation on Pt-Cu single-atom alloys. ACS Catal 7:413–420. https://doi.org/10.1021/acscatal.6b02772
44. Mon M, Ferrando-Soria J, Grancha T et al (2016) Selective gold recovery and catalysis in a highly flexible methionine-decorated metal-organic framework. J Am Chem Soc 138:7864–7867. https://doi.org/10.1021/jacs.6b04635

45. Mon M, Rivero-Crespo MA, Ferrando-Soria J et al (2018) synthesis of densely packaged, ultrasmall Pt02 clusters within a thioether-functionalized mof: catalytic activity in industrial reactions at low temperature. Angew Chemie, Int Ed 57:6186–6191. https://doi.org/10.1002/anie.201801957
46. Murahashi T, Fujimoto M, Oka M (2006) discrete sandwich compounds of monolayer palladium sheets. Science (80) 313:1104 LP–1107. https://doi.org/10.1126/science.1125245
47. Murahashi T, Kato N, Uemura T, Kurosawa H (2007) Rearrangement of a Pd4 skeleton from a 1D chain to a 2D sheet on the face of a perylene or fluoranthene ligand caused by exchange of the binder molecule. Angew Chemie Int Ed 46:3509–3512. https://doi.org/10.1002/anie.200700340
48. Murahashi T, Uemura T, Kurosawa H (2003) Perylene − Tetrapalladium Sandwich Complexes. J Am Chem Soc 125:8436–8437. https://doi.org/10.1021/ja0358246
49. Oliver-Meseguer J, Cabrero-Antonino JR, Dominguez I (2012) Small gold clusters formed in solution give reaction turnover numbers of 107 at room temperature. Sci (Washington, DC, United States) 338:1452–1455. https://doi.org/10.1126/science.1227813
50. Oliver-Meseguer J, Dominguez I, Gavara R (2017) The wet synthesis and quantification of ligand-free sub-nanometric Au clusters in solid matrices. Chem Commun (Cambridge, United Kingdom) 53:1116–1119. https://doi.org/10.1039/C6CC09119A
51. Oliver-Meseguer J, Dominguez I, Gavara R et al (2017) Disassembling Metal Nanocrystallites into Sub-nanometric Clusters and Low-faceted Nanoparticles for Multisite Catalytic Reactions. Chem Cat Chem 9:1429–1435. https://doi.org/10.1002/cctc.201700037
52. Oliver-Meseguer J, Leyva-Perez A, Al-Resayes SI, Corma A (2013) Formation and stability of 3–5 atom gold clusters from gold complexes during the catalytic reaction: dependence on ligands and counteranions. Chem Commun (Cambridge, United Kingdom) 49:7782–7784. https://doi.org/10.1039/c3cc44104k
53. Oliver-Meseguer J, Leyva-Perez A, Corma A (2013) Very small (3–6 atoms) gold cluster catalyzed carbon-carbon and carbon-heteroatom bond-forming reactions in solution. Chem Cat Chem 5:3509–3515. https://doi.org/10.1002/cctc.201300695
54. Oliver-Meseguer J, Liu L, Garcia-Garcia S et al (2015) Stabilized naked sub-nanometric cu clusters within a polymeric film catalyze C-N, C-C, C-O, C-S, and C-P Bond-Forming Reactions. J Am Chem Soc 137:3894–3900. https://doi.org/10.1021/jacs.5b03889
55. Panyala RN, Pena-Mendez ME, Havel J (2009) Gold and nano-gold in medicine: overview, toxicology and perspectives. J Appl Biomed 7:75–91
56. Pastoriza-Santos I, Liz-Marzan LM (1999) Formation and stabilization of silver nanoparticles through reduction by N, N-dimethylformamide. Langmuir 15:948–951. https://doi.org/10.1021/LA980984U
57. Peredkov S, Peters S, Al-Hada M et al (2016) Structural investigation of supported Cun clusters under vacuum and ambient air conditions using EXAFS spectroscopy. Catal Sci Technol 6:6942–6952. https://doi.org/10.1039/C6CY00436A
58. Polozkov RG, Ivanov VK, Verkhovtsev AV (2013) New applications of the jellium model for the study of atomic clusters. J. Phys. Conf. Ser. 438. https://doi.org/10.1088/1742-6596/438/1/012009
59. Rivero-Crespo MA, Leyva-Pérez A, Corma A (2017) A ligand-free Pt 3 cluster catalyzes the markovnikov hydrosilylation of alkynes with up to 10 6 turnover frequencies. Chem - A Eur J 23:1702–1708. https://doi.org/10.1002/chem.201605520
60. Rivero-Crespo MA, Mon M, Ferrando-Soria J et al (2018) Confined Pt11 + water clusters in a MOF catalyze the low-temperature water-gas shift reaction with both CO_2 oxygen atoms coming from water. Angew Chemie, Int Ed 57:17094–17099. https://doi.org/10.1002/anie.201810251
61. Rubio-Marques P, Rivero-Crespo MA, Leyva-Perez A, Corma A (2015) Well-defined noble metal single sites in zeolites as an alternative to catalysis by insoluble metal salts. J Am Chem Soc 137:11832–11837. https://doi.org/10.1021/jacs.5b07304
62. Sa J, Frances S, Taylor R (2012) Redispersion of gold supported on oxides

63. Sá J, Goguet A, Taylor SFR et al (2011) Influence of methyl halide treatment on gold nanoparticles supported on activated carbon. Angew Chem Int Ed Engl 50:8912–8916. https://doi.org/10.1002/anie.201102066
64. Sakaki S, Mizoe N, Sugimoto M (1998) theoretical study of platinum(0)-catalyzed hydrosilylation of ethylene. chalk − harrod mechanism or modified chalk − harrod mechanism. Organometallics 17:2510–2523. https://doi.org/10.1021/om980190a
65. Scarabelli L, Coronado-Puchau M, Giner-Casares JJ et al (2014) monodisperse gold nanotriangles: size control, large-scale self-assembly, and performance in surface-enhanced raman scattering. ACS Nano 8:5833–5842. https://doi.org/10.1021/nn500727w
66. Serna P, Gates BC (2014) Molecular metal catalysts on supports: organometallic chemistry meets surface science. Acc Chem Res 47:2612–2620. https://doi.org/10.1021/ar500170k
67. Sharma S, Kurashige W, Niihori Y, Negishi Y (2016) Nanocluster Science. Elsevier Inc
68. Tian S, Fu Q, Chen W et al (2018) Carbon nitride supported Fe2 cluster catalysts with superior performance for alkene epoxidation. Nat Commun 9:2353. https://doi.org/10.1038/s41467-018-04845-x
69. Vajda S, White MG (2015) Catalysis applications of size-selected cluster deposition. ACS Catal 5:7152–7176. https://doi.org/10.1021/acscatal.5b01816
70. Wang N, Sun Q, Yu J (2019) Ultrasmall metal nanoparticles confined within crystalline nanoporous materials: a fascinating class of nanocatalysts. Adv Mater 31:1–23. https://doi.org/10.1002/adma.201803966
71. Wu X-F, Anbarasan P, Neumann H, Beller M (2010) From noble metal to nobel prize: palladium-catalyzed coupling reactions as key methods in organic synthesis. Angew Chemie, Int Ed 49:9047–9050. https://doi.org/10.1002/anie.201006374
72. Yang Y, Reber AC, Gilliland SE et al (2018) Donor/acceptor concepts for developing efficient suzuki cross-coupling catalysts using graphene-supported Ni, Cu, Fe, Pd, and Bimetallic Pd/Ni Clusters. J Phys Chem C 122:25396–25403. https://doi.org/10.1021/acs.jpcc.8b07538
73. Zea H, Lester K, Datye AK et al (2005) The influence of Pd-Ag catalyst restructuring on the activation energy for ethylene hydrogenation in ethylene-acetylene mixtures. Appl Catal A Gen 282:237–245. https://doi.org/10.1016/j.apcata.2004.12.026
74. Zhai Y, Pierre D, Si R (2010) Alkali-stabilized Pt-OH_x species catalyze low-temperature water-gas shift reactions. Science (80) 329:1633 LP–1636. https://doi.org/10.1126/science.1192449
75. Zhang C, Laine RM (2000) Hydrosilylation of allyl alcohol with [HSiMe2OSiO1.5]8: Octa (3-hydroxypropyldimethylsiloxy) octasilsesquioxane and its octamethacrylate derivative as potential precursors to hybrid nanocomposites. J Am Chem Soc 122:6979–6988. https://doi.org/10.1021/ja000318r
76. Zitoun D, Respaud M, Fromen M-C et al (2002) Magnetic enhancement in nanoscale corh particles. Phys Rev Lett 89:37203. https://doi.org/10.1103/PhysRevLett.89.037203